MOLECULAR AND CELLULAR BIOLOGY, Sept. 2011, p. 3745–3758 Vol. 31, No. 18
0270-7306/11/$12.00 doi:10.1128/MCB.05303-11

Requirement of FADD, NEMO, and BAX/BAK for Aberrant Mitochondrial Function in Tumor Necrosis Factor Alpha-Induced Necrosis▽

Krishna M. Irrinki,[1]† Karthik Mallilankaraman,[1]† Roshan J. Thapa,[2] Harish C. Chandramoorthy,[1] Frank J. Smith,[1] Neelakshi R. Jog,[3] Rajesh Kumar Gandhirajan,[1] Steven G. Kelsen,[3] Steven R. Houser,[4] Michael J. May,[5] Siddharth Balachandran,[2] and Muniswamy Madesh[1]*

Department of Biochemistry, Temple University, Philadelphia, Pennsylvania 19140[1]; Immune Cell Development & Host Defense Program, Fox Chase Cancer Center, Philadelphia, Pennsylvania 19111[2]; Department of Medicine, Temple University, Philadelphia, Pennsylvania 19140[3]; Department of Physiology, Temple University, Philadelphia, Pennsylvania 19140[4]; and Department of Animal Biology, University of Pennsylvania School of Veterinary Medicine, Philadelphia, Pennsylvania 19104[5]

Received 4 March 2011/Returned for modification 28 March 2011/Accepted 26 June 2011

Necroptosis represents a form of alternative programmed cell death that is dependent on the kinase RIP1. RIP1-dependent necroptotic death manifests as increased reactive oxygen species (ROS) production in mitochondria and is accompanied by loss of ATP biogenesis and eventual dissipation of mitochondrial membrane potential. Here, we show that tumor necrosis factor alpha (TNF-α)-induced necroptosis requires the adaptor proteins FADD and NEMO. FADD was found to mediate formation of the TNF-α-induced pronecrotic RIP1-RIP3 kinase complex, whereas the IκB Kinase (IKK) subunit NEMO appears to function downstream of RIP1-RIP3. Interestingly, loss of RelA potentiated TNF-α-dependent necroptosis, indicating that NEMO regulates necroptosis independently of NF-κB. Using both pharmacologic and genetic approaches, we demonstrate that the overexpression of antioxidants alleviates ROS elevation and necroptosis. Finally, elimination of BAX and BAK or overexpression of Bcl-x_L protects cells from necroptosis at a later step. These findings provide evidence that mitochondria play an amplifying role in inflammation-induced necroptosis.

Eukaryotic cells undergo cell death in multiple pathways, including by necrosis and apoptosis. Necrosis is induced as a result of direct or indirect damage to the plasma membrane with subsequent loss of cytoplasmic components, perturbation of ion homeostasis, rapid swelling, and lysis (49). Necrosis occurs in nonphysiological settings, coordinately in groups of adjacent cells, and in connection with inflammation (64). In contrast, apoptosis is a physiological process that takes place in noncontiguous cells and is generally not associated with inflammation (20, 56). Apoptotic cells exhibit a condensed nuclear structure, compacted cytoplasmic organelles, plasma membrane blebbing, and a decrease in cell size (17). Apoptotic signaling proceeds via well-defined extrinsic and intrinsic pathways (12, 69). The extrinsic pathways of apoptosis are initiated by members of the death receptor family of transmembrane proteins that regulate a membrane-proximal death-inducing signaling complex (DISC). The DISC triggers activation of caspase 8 to initiate an enzymatic cascade that mediates ordered apoptotic dismantling of the target cell (6, 51). On the other hand, when cells are challenged with the death receptor ligands tumor necrosis factor alpha (TNF-α), FasL, or TNF-related apoptosis-inducing ligand (TRAIL) in the presence of caspase inhibitors, a newly described cell death process called necroptosis is induced (10, 28, 29, 65, 72). Necroptosis is also triggered by bacterial toxins and viral infection (63). Necroptotic cell death initiated by TNF-α, Fas, or TRAIL is mediated by formation of a complex of two kinases, RIP1 and RIP3. This complex promotes mitochondrial reactive oxygen species (ROS) production and eventual collapse of cellular energy production (10, 14, 72). The RIP1-RIP3 complex appears to promote ATP depletion during necroptosis by impinging on components of the mitochondrial permeability transition pore (PTP) (28, 62), although the molecular details are unknown. Furthermore, the relationships between ROS production and compromised cell bioenergetics are not understood.

ROS are produced primarily by two distinct mechanisms. One source of ROS is the ubiquitously expressed NADPH oxidase (NOX)-family proteins that interact with regulatory adaptor proteins and promote the generation of extra- and intracellular superoxides (36). A second major source of ROS is derived from mitochondrial oxidative phosphorylation (19, 25). Under conditions associated with excess production of ROS, such as inflammation or ischemic reperfusion (IR), the rate of ROS generation by tissues can exceed the capacity of endogenous oxidant defense mechanisms to detoxify ROS and prevent deleterious radical-mediated reactions (8). Whereas ROS elevation has been speculated to contribute to necroptosis, the source(s) and roles of ROS remain elusive.

Murine embryonic fibroblasts (MEFs) undergo necroptosis in response to a variety of stimuli, including the combination of TNF-α–cycloheximide (CHX)–zVAD (TCZ) (10). Here, we show that, in addition to RIP1 and RIP3, the adaptor proteins FADD and NEMO are also crucial for TNF-α-induced

* Corresponding author. Mailing address: Department of Biochemistry, Temple University, 627 Kresge Building, 3440 N. Broad Street, Philadelphia, PA 19140. Phone: (215) 707-5465. Fax: (215) 707-7536. E-mail: madeshm@temple.edu.
† These authors contributed equally to the manuscript.
▽ Published ahead of print on 11 July 2011.

necroptosis. The formation of TNF-α-induced RIP1-RIP3 necroptotic complex is independent of cytosolic Ca^{2+}. We also show that the pro-cell-death Bcl-2-family proteins BAX and BAK are required for mitochondrial dysfunction in response to necroptotic agonists, while overexpression of Bcl-x_L is protective. It is also evident that the ROS plays a crucial role in TCZ-induced mitochondrial dysfunction. Further, our results demonstrate that FADD-RIP1-RIP3-mediated mitochondrial malfunction is dependent on TNF-α signaling molecule NEMO, a previously undescribed key mediator of cytokine-induced necroptosis. We propose that a FADD-RIP1-RIP3-NEMO complex induces BAX/BAK-dependent disintegration of mitochondrial bioenergetics to promote TNF-α-driven necroptosis.

MATERIALS AND METHODS

Wild-type (WT), FADD-knockout (KO) ($FADD^{-/-}$), $RIP1^{-/-}$, caspase $8^{-/-}$ MEFS, BAD/BAK-double-knockout (DKO) ($BAX^{-/-}$ $BAK^{-/-}$), $NEMO^{-/-}$, and $RelA^{-/-}$ MEFs were grown in Dulbecco's modified Eagle's medium (DMEM) supplemented with 10% fetal bovine serum (FBS), 100 U/ml penicillin, and 100 μg/ml streptomycin. $FADD^{-/-}$ and FADD MEFs were cultured in Dulbecco's modified Eagle's medium supplemented with 10% FBS, 100 U/ml penicillin, and 100 μg/ml streptomycin. For treatment of cells, mouse TNF-α (25 ng/ml; R&D Systems), cycloheximide (0.250 μg/ml; Sigma), and zVAD-FMK (50 μM; BD Biosciences) were used throughout the study. All the treatments were for 20 h, unless specified.

Mitochondrial oxygen consumption rate. MEFs (2.5×10^6 cells) were permeabilized by 0.01% digitonin in intracellular medium (ICM) buffer (120 mM KCl, 10 mM NaCl, 1 mM KH_2PO_4, 20 mM HEPES–Tris, pH 7.2) and placed into a MT200A Mitocell chamber, and oxygen consumption was measured in nanomoles O_2 via a Clark-type electrode (StrathKelvin Instruments) (26). After the chamber was sealed, successive additions of malate (5 mM)–pyruvate (5 mM), rotenone (100 nM), succinate (5 mM), antimycin A (50 nM), tetramethyl-*p*-phenylenediamine (TMPD; 0.4 mM)–ascorbate (2.5 mM), and the complex IV inhibitor sodium azide were made under constant stirring in 30-s intervals via a Hamilton syringe. The rate of oxygen consumption was measured and is displayed as nanomoles oxygen/min/2.5×10^6 cells, and the values represent azide-sensitive oxygen consumption.

Simultaneous confocal visualization of $\Delta\Psi_m$ and plasma membrane integrity. MEFs cultured on glass-bottom dishes were treated with TCZ for the indicated time periods. After treatment, the cells were incubated with 100 nm tetramethylrhodamine ethyl ester perchlorate (TMRE; a mitochondrial membrane potential [$\Delta\Psi_m$] indicator; Invitrogen) in the dark for 20 min at 37°C. To assess plasma membrane integrity, nuclear dye TOTO-3 iodide (1:1,400; Molecular Probes) was also applied during TMRE loading for 10 min. Images were acquired using a Carl Zeiss 510 Meta confocal system with excitations at 561 nm and 633 nm for mitochondrial membrane potential and plasma membrane integrity, respectively (47). Five images were randomly collected for each sample, and perinuclear fluorescence change was quantified using ImageJ software. Fluorescent tracings are representative of the mean fluorescence value of all cells in one field and are indicative of at least three independent experiments. Data are presented as the means ± standard errors of the means (SEMs).

ATP measurements. Cells were grown in a 12-well plate and treated with TCZ for 20 h in quadruplicate. Samples for ATP measurements were prepared using a CellTiter-Glo luminescent cell viability assay kit (Promega) according to the manufacturer's instructions. ATP levels (luminescence) were measured in a model 96 F nontreated white microwell plate (Nunc) using a Victor X5 2030 multilabel reader (Perkin Elmer). The readout was normalized to that for untreated controls and analyzed using Sigma Plot software.

Cell permeabilization and preparation of cytosol/mitochondrion-enriched pellet. MEFs (7×10^6) treated with TCZ for the indicated time periods were trypsinized, resuspended, and permeabilized with 40 μg/ml digitonin in 1.5 ml of ICM buffer supplemented with protease inhibitors and phenylmethylsulfonyl fluoride (1 mM). To lower ambient Ca^{2+}, all buffers used for $\Delta\Psi_m$ and biochemical assays were passed through a metal-chelating Bio-Rad Chelex-100 cation-exchange column before the experiments were performed. Ca^{2+}-free ICM buffer was prepared with a Chelex column before the addition of protease inhibitors. For cytosol swap experiments, equal numbers of MEFs (7×10^6) treated with TCZ for the indicated time periods were trypsinized, resuspended, and permeabilized with 40 μg/ml digitonin in 1.5 ml of ICM buffer for 7 min, and the effectiveness of permeabilization was evaluated by trypan blue exclusion. Permeabilized cells were centrifuged at 20,000 rpm for 5 min at 4°C. The supernatant containing cytosol and the pellet containing mitochondria were collected and used immediately. The entire volume of cytosol was utilized for cytosol swap experiments (44).

Subcellular fractionation. MEFs were homogenized in mitochondrion isolation buffer (3 mM HEPES, 10 mM KCl, 1.5 mM $MgCl_2$, 0.5 mM EDTA, 1 mM EGTA, 230 mM mannitol, 70 mM sucrose, pH 7.5, 1 mM dithiothreitol, and 0.1 mM phenylmethylsulfonyl fluoride with protease inhibitor mix). The homogenate was centrifuged at $800 \times g$, and the nuclear and cell debris was removed. The supernatant was centrifuged at $10{,}000 \times g$, and the resultant pellet was further processed for mitochondrion purification over a Percoll gradient. The postmitochondrial supernatant was subjected to $100{,}000 \times g$, and the microsomal pellet and cytosolic supernatants were collected separately (46).

$\Delta\Psi_m$ measurements. Fluorescence was monitored in a multiwavelength excitation dual-wavelength emission fluorimeter (Delta RAM; Photon Technology International) with 490-nm excitation/535-nm emission for the monomeric form (JC-1; Molecular Probes) and 570-nm excitation/595-nm emission for the J aggregate of JC-1. $\Delta\Psi_m$ was measured as the ratio of the fluorescence of the J-aggregate (aqueous phase) and monomer (membrane-bound) forms of JC-1 (43).

Flow cytometric analysis of intracellular ROS levels. Cells were treated with TCZ for 20 h. For ROS measurement, cells were stained with an oxidation-sensitive dye, 2′,7′-dichlorofluorescein diacetate (H_2DCF-DA; 10 μM; Molecular Probes), and dihydroethidine (DHE; 10 μM; Molecular Probes) (27) in DMEM for 20 min at 37°C (45). The cells were analyzed on a FACSCanto apparatus (BD Biosciences). Relative fluorescence intensities were plotted on a logarithmic scale using Flow-Jo software.

Adenoviral infection. Studies used similar multiplicities of infection (MOIs) to test recombinant manganese superoxide dismutase (MnSOD) and glutathione peroxidase 1 (GPX1) adenovirus 5 (Ad5)-cytomegalovirus (CMV) vectors (Ad5CMVSOD2 and Ad5CMVGPX1; University of Iowa Gene Transfer Core). Cells were infected with Ad5CMVSOD2 or Ad5CMVGPX1 at an MOI of 2,000 particles/cell as described previously (14).

Immunoprecipitation and Western blotting. MEFs (1×10^6/condition) were cultured in 10-cm dishes and treated with TCZ for the indicated times in the presence or absence of necrostatin-1 (Nec-1; 25 μM). Cells were harvested, lysed, and sonicated for 5 s (lysis buffer, 1% Triton X-100, 150 mM NaCl, 20 mM HEPES [pH 7.3], 5 mM EDTA, 5 mM NaF, 0.2 mM $NaVO_3$ [*ortho*], and complete protease inhibitor cocktail [Roche]). Lysates were clarified by centrifugation (14,000 rpm for 10 min at 4°C), and anti-RIP3 antibody (2 μg) was added to each sample. After overnight incubation at 4°C, samples were supplemented with protein A/G-agarose slurry (40 μl) and incubated for an additional 2 h. Immunoprecipitates were washed four times with cold lysis buffer and eluted by directly boiling the agarose beads in SDS sample buffer. The samples were subjected to 10% SDS-PAGE, and Western blotting was performed.

Immunocytochemistry. MEFs cultured on 25-mm glass coverslips were treated with TCZ for 6 h. Cells were then fixed with 3% paraformaldehyde and permeabilized with digitonin (200 μg/ml). Cells were probed for anti-cytochrome *c* antibody (catalog no. 556433; BD Pharmingen), Smac/Diablo antibody (abcam8115), HtrA2/Omi antibody (ab64111), and apoptosis-inducing factor (AIF) antibody (catalog no. 4642; Cell Signaling Technology) and visualized using an Alexa Fluor-488 secondary antibody (Invitrogen). Hoechst 33342 was used as a nuclear stain. Images were acquired by confocal microscopy. Mitochondrial intermembrane space (IMS) protein fluorescence was quantitated using ImageJ software (version 1.44).

RESULTS

TNF-α-induced necroptotic signal targets mitochondrial respiration. Inhibition of TNF-α–CHX-induced apoptosis by caspase inhibitors (zVAD) triggers a divergent form of cell death called necroptosis, characterized by loss of ATP and elevated ROS levels (10, 28). Although necroptosis is evident in pathological settings, including ischemia/reperfusion injury, sepsis, acute pancreatitis, and viral inflammation, the links between the necroptotic signaling cascade and mitochondrial dysfunction are poorly understood. To investigate the role of mitochondrial bioenergetics in necroptosis, we measured oxy-

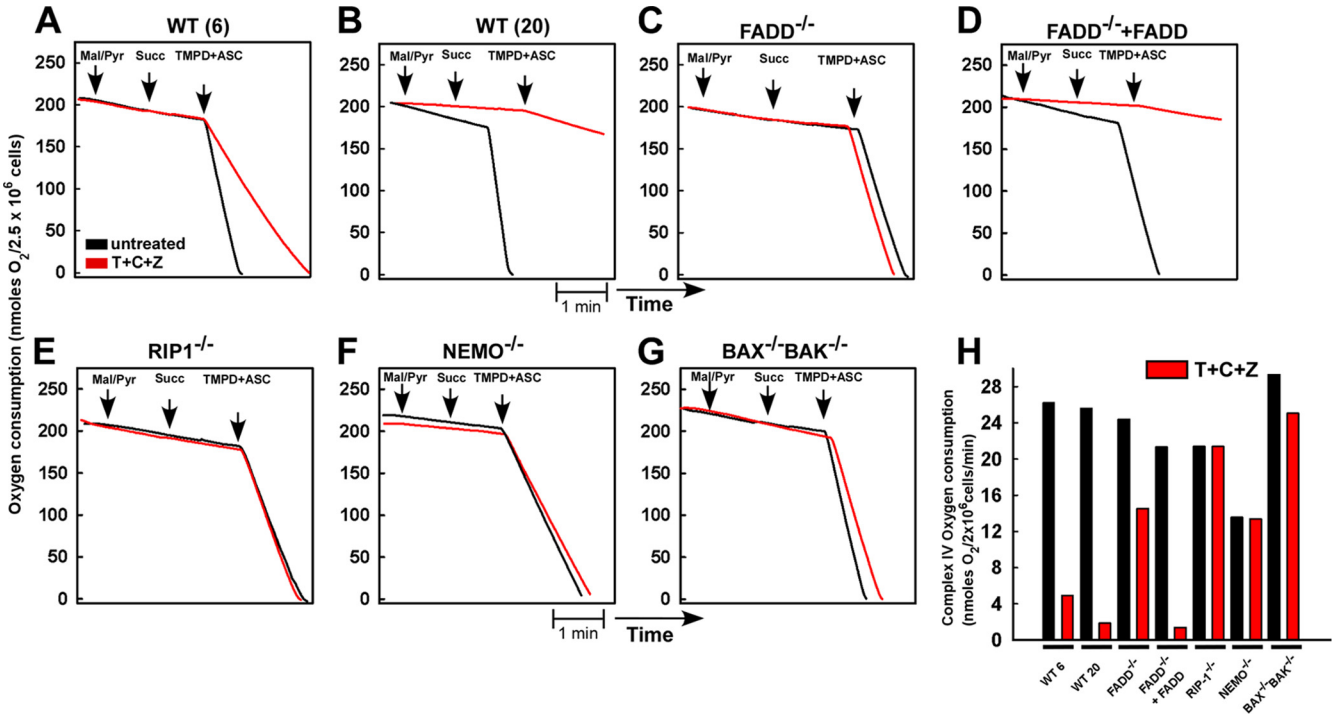

FIG. 1. TNF-α–CHX–zVAD challenge results in FADD-, RIP1-, NEMO-, and BAX/BAK-dependent reduction of mitochondrial oxygen consumption. (A) Determination of mitochondrial oxygen consumption by a Clark-type electrode in wild-type MEFs challenged with or without TNF-α (25 ng/ml)–cycloheximide (0.25 μg/ml)–zVAD (50 μM) (TCZ) for 6 h. For the following experiments, MEFs were challenged with TCZ for 20 h. (B to G) Wild-type (B), FADD$^{-/-}$ (C), FADD$^{-/-}$ FADD (D), RIP1$^{-/-}$ (E), NEMO$^{-/-}$ (F), and BAX$^{-/-}$ BAK$^{-/-}$ (G) MEFs. These cells were then permeabilized with intracellular medium buffer containing digitonin (40 μg/ml). Mitochondrial complex I (malate/pyruvate [Mal/Pyr]; 5 mM), II (succinate [Succ]; 5 mM), and IV (TMPD at 0.4 mM plus ascorbate [ASC] at 2.5 mM) substrates were subsequently added to the closed chamber, and the rate of oxygen consumption was measured. Black traces, untreated samples; red traces, representative results for samples treated for 20 h with TCZ. MEFs were pretreated with CHX (0.25 μg/ml) plus zVAD-FMK (50 μM) for 1 h prior to TNF-α stimulation. (H) Quantitation of mitochondrial respiratory complex IV oxygen consumption rate following TCZ treatment. Oxygen consumption was measured using TMPD-ascorbate as the electron donor, and the results of the analysis are expressed as complex IV oxygen consumption (nanomoles $O_2/2.0 \times 10^6$ cells/min). Note that the rate of oxygen consumption by complexes I and II was reduced at 20 h but not 6 h of TCZ challenge in wild-type MEFs. Black traces, untreated samples; red traces, representative results for samples treated with TCZ. The bar graph represents means ± SEMs of at least three independent experiments.

gen consumption rates in permeabilized cells after challenging murine embryonic fibroblasts with TCZ (Fig. 1). Treatment of wild-type MEFs with TCZ for 6 h was associated with a decrease in oxygen consumption that was exacerbated by 20 h of treatment (Fig. 1A, B, and H). Upon TNF-α stimulation, the TNFR1 signaling complex recruits FADD, RIP1, and caspase 8 to activate apoptosis or necrosis (28, 38, 42, 68). We therefore examined whether the absence of either FADD or RIP1 affected mitochondrial oxygen consumption following TCZ treatment. Oxygen consumption in FADD- or RIP1-deficient MEFs was unaffected in response to TCZ (Fig. 1C, E, and H). Importantly, stable reexpression of full-length FADD in FADD$^{-/-}$ MEFs rescued the wild-type phenotype (Fig. 1D and H). Activation of NF-κB by TNF-α requires an IκB kinase (IKK) complex that is comprised of two catalytic subunits (IKKα and IKKβ) and a crucial regulatory subunit, NEMO (21, 31). To determine whether NF-κB-driven signaling plays a role in necroptosis, MEFs lacking NEMO were challenged with TCZ. NEMO$^{-/-}$ MEFs had similar rates of oxygen consumption as untreated cells (Fig. 1F and H), suggesting that NEMO is required for TCZ-induced necroptosis. BAX and BAK play major roles in apoptosis by impinging on mitochondria (53, 60, 70). We found that MEFs deficient in both BAX and BAK were resistant to TCZ-induced reduction of oxygen consumption (Fig. 1G and H), implicating these proteins in the necroptosis pathway. Together, these results indicate that FADD, RIP1, NEMO, and BAX/BAK are necessary for the altered mitochondrial respiration that occurs during necroptosis.

Loss of mitochondrial membrane potential is associated with TNF-α-induced necroptosis. Mitochondria play a crucial role in both apoptosis and necrosis via mitochondrial intermembrane resident protein release and opening of the mitochondrial permeability transition pore, respectively (22). We examined whether the decline of mitochondrial oxygen consumption observed in necroptosis in response to TCZ was associated with a collapse of $\Delta\Psi_m$. After TCZ challenge, $\Delta\Psi_m$ was measured in permeabilized MEFs using a ratiometric potential indicator, JC-1. TCZ treatment of wild-type MEFs caused a robust loss of $\Delta\Psi_m$ (Fig. 2A and H). The loss of $\Delta\Psi_m$ was completely prevented in FADD-, RIP1-, NEMO-, and BAX/BAK-deficient MEFs (Fig. 2B, D, F, G, and H). Reexpression of FADD in FADD$^{-/-}$ cells restored the sensitivity of $\Delta\Psi_m$ to TCZ (Fig. 2C and H). Binding of apoptosis-inducing

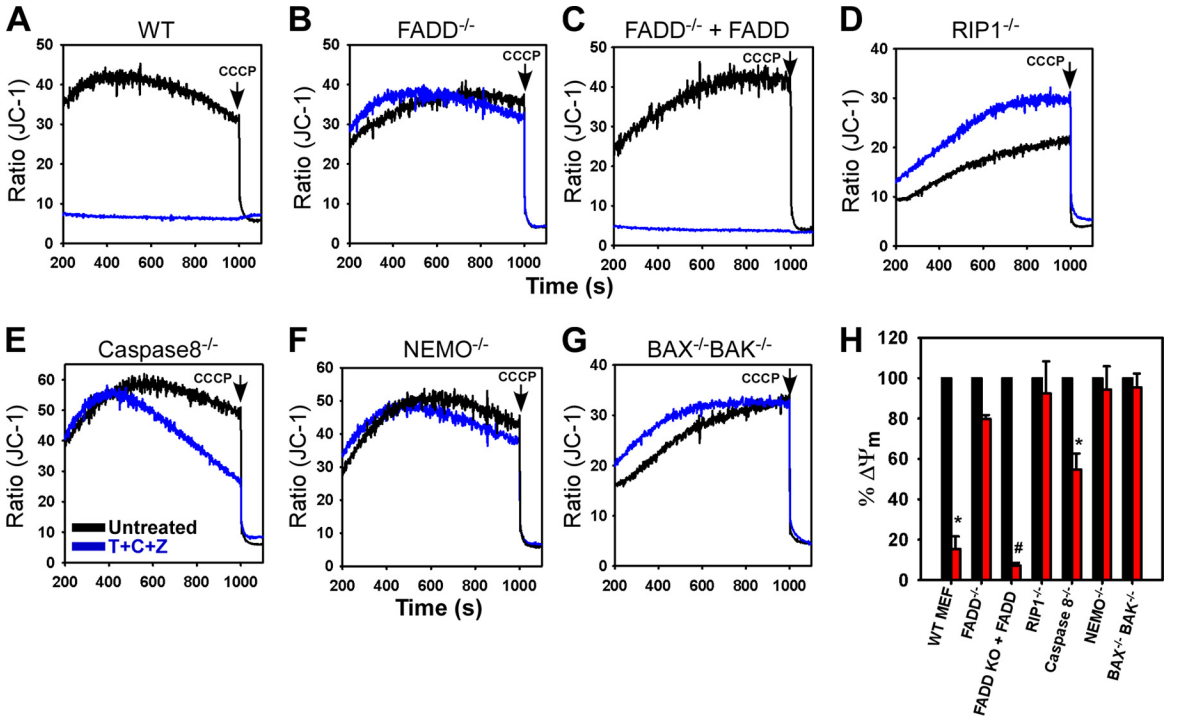

FIG. 2. Disruption of mitochondrial membrane potential gradient in TNF-α-induced necroptosis requires FADD, RIP1, NEMO, and BAX/BAK. MEFs were treated with dimethyl sulfoxide or TCZ for 20 h. Permeabilized cells were loaded with the ratiometric mitochondrial membrane potential indicator JC-1, and $\Delta\Psi_m$ was examined for 18 min. At 1,000 s, cells were challenged with a mitochondrial uncoupler (carbonyl cyanide *m*-chlorophenylhydrazone [CCCP]; 2 μM) to dissipate the total $\Delta\Psi_m$. (A) Wild-type cells challenged with TCZ induced a large $\Delta\Psi_m$ loss. (B) FADD$^{-/-}$ MEFs were resistant to TCZ-induced $\Delta\Psi_m$ loss. (C) In contrast, reintroduction of full-length FADD in FADD$^{-/-}$ MEFs reestablished the $\Delta\Psi_m$ loss in response to TCZ challenge. (D) Similarly, RIP1$^{-/-}$ MEFs failed to undergo $\Delta\Psi_m$ loss after TCZ treatment. (E) TCZ challenge partially affected the caspase 8$^{-/-}$ MEFs $\Delta\Psi_m$ gradient. NEMO$^{-/-}$ MEF (F) and BAX$^{-/-}$ BAK$^{-/-}$ MEF (G) $\Delta\Psi_m$ was unaffected by TCZ challenge. (H) Quantitation of $\Delta\Psi_m$ maintenance in MEFs before and after TCZ treatment. Data are represented as means ± SEMs from three to six independent experiments.

cytokines, including Fas, TRAIL, and TNF-α, to their cognate receptors facilitates recruitment of FADD and pro-caspase 8 to form a death-inducing complex. The FADD-caspase 8 complex promotes mitochondrion-dependent apoptosis via processing of the Bcl-2 family member BID. Having demonstrated that TNF-α is capable of inducing cell death via two distinct caspase 8 activation pathways (68), we examined the contribution of caspase 8 to necroptosis. Although it was not prevented, the normal loss of $\Delta\Psi_m$ induced by TCZ was delayed in caspase 8$^{-/-}$ MEFs (Fig. 2E and H). These results confirm that the decline of mitochondrial oxygen consumption observed in the necroptotic response to TCZ was associated with a collapse of $\Delta\Psi_m$ associated with a necroptosis signaling complex involving FADD and RIP1.

Requirement of BAX and BAK for TNF-α-induced necroptosis. To further examine whether the necroptosis signaling complex targets mitochondria for bioenergetic collapse, mitochondrion-enriched pellets from untreated wild-type MEFs were exposed to cytosol prepared from either untreated or TCZ-treated FADD$^{-/-}$, FADD$^{-/-}$ FADD, RIP1$^{-/-}$, caspase 8$^{-/-}$, NEMO$^{-/-}$, and BAX$^{-/-}$ BAK$^{-/-}$ MEFs, and the $\Delta\Psi_m$ was monitored. Cytosol from wild-type untreated cells was without effect on $\Delta\Psi_m$, whereas that from TCZ-treated cells caused a reduction of $\Delta\Psi_m$ (Fig. 3A and H). In contrast, cytosol prepared from TCZ-challenged FADD$^{-/-}$, RIP1$^{-/-}$, and NEMO$^{-/-}$ MEFs had only a minimal effect on $\Delta\Psi_m$ (Fig. 3B, D, F, and H). In similar experiments with FADD reexpressed in FADD$^{-/-}$ MEFs, the TCZ-treated cytosol induced a $\Delta\Psi_m$ loss similar to that in the wild type (Fig. 3C and H). Cytosol from TCZ-treated caspase 8$^{-/-}$ cells induced a slower but considerable $\Delta\Psi_m$ loss (Fig. 3E and H). Cytosol from TCZ-challenged BAX$^{-/-}$ BAK$^{-/-}$ cells are capable of stimulating complete wild-type $\Delta\Psi_m$ loss (Fig. 3G and H). Together, these results show that BAX/BAK likely contributes to necroptosis via mitochondrial depolarization.

Inhibition of RIP1 prevents mitochondrial dysfunction and TNF-α-induced necroptosis. To verify the role of TNF-α signaling molecules in mitochondrial dysfunction and cell death, we translated our experimental approach to intact cells. We first tested whether a necroptotic complex exists after TCZ challenge in the absence of either FADD or RIP1. RIP3 was immunoprecipitated from wild-type cells, and the immune complex was examined by Western blotting using anti-FADD and anti-RIP1 antibodies. Both RIP1 and FADD coprecipitated with RIP3. The level of interaction was elevated after 4 and 6 h of TCZ treatment (Fig. 4A). The selective allosteric RIP1 inhibitor Nec-1 interferes with the RIP1-RIP3 interaction (15, 16). Pretreatment with Nec-1 disrupted the association of FADD with RIP1 and RIP3 in the cells exposed to TCZ (Fig. 4A). In addition, there was only a minimal interaction of

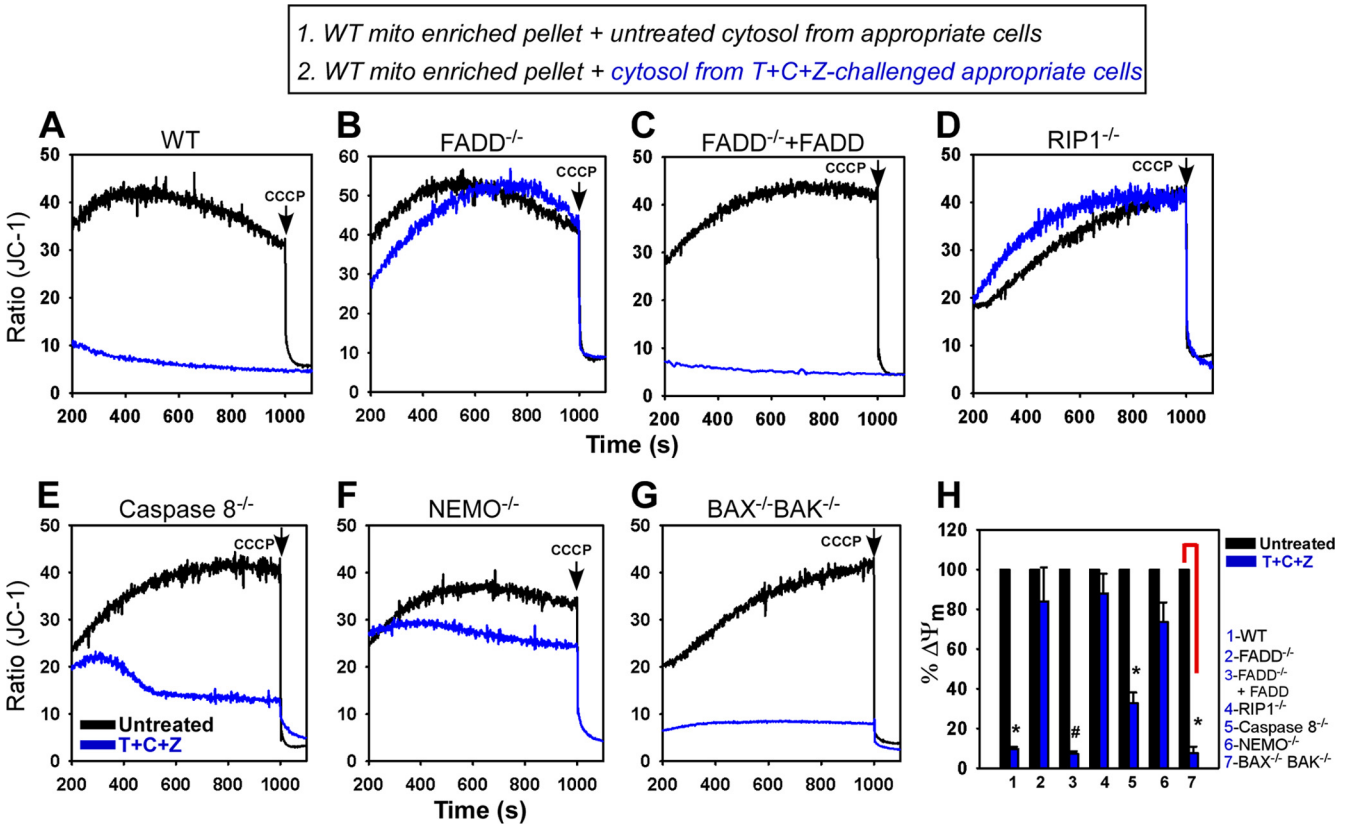

FIG. 3. Proximal candidates FADD, RIP1, and NEMO are required for depolarization of mitochondrial membrane during necroptosis. MEFs were challenged for 20 h with TCZ or dimethyl sulfoxide. To perform cytosol exchange experiments, TCZ-treated wild-type (A), FADD$^{-/-}$ (B), FADD$^{-/-}$ FADD (C), RIP1$^{-/-}$ (D), caspase 8$^{-/-}$ (E), NEMO$^{-/-}$ (F), and BAX$^{-/-}$ BAK$^{-/-}$ (G) cells were permeabilized for 6 min with intracellular medium containing digitonin (40 μg/ml). The cytosol was prepared after centrifugation at 20,000 rpm for 5 min. Similarly, a wild-type mitochondrion-enriched pellet was prepared for cytosol swap experiments. Wild-type $\Delta\Psi_m$ was unaffected by the cytosol from FADD$^{-/-}$ (B), RIP1$^{-/-}$ (D), and NEMO$^{-/-}$ (F) TCZ-challenged MEFs. (E) Although $\Delta\Psi_m$ was maintained at the earlier time point, caspase 8$^{-/-}$ cytosol also elicited a considerable amount of wild-type $\Delta\Psi_m$ loss. In sharp contrast, cytosol from the FADD-reconstituted FADD$^{-/-}$ cells induced complete $\Delta\Psi_m$ loss (C). Interestingly, TCZ-treated BAX$^{-/-}$ BAK$^{-/-}$ cytosol induced a substantial amount of wild-type $\Delta\Psi_m$ loss. (H) Quantitation of wild-type $\Delta\Psi_m$ preservation after cytosol exchange. The results in panel H are representative of three to six independent experiments.

RIP1 and RIP3 present in TCZ-treated FADD$^{-/-}$ MEFs. Furthermore, coimmunoprecipitation experiments suggested that the interaction between FADD and RIP3 was disrupted in RIP1$^{-/-}$ cells (Fig. 4A). These results suggest that FADD and RIP3 do not interact directly; instead, RIP1 likely recruits FADD to RIP3 for necroptotic complex formation.

To further confirm the role of mitochondria in TNF-α-induced necroptosis, we treated wild-type, FADD$^{-/-}$, FADD$^{-/-}$ FADD, RIP1$^{-/-}$, caspase 8$^{-/-}$, NEMO$^{-/-}$, and BAX$^{-/-}$ BAK$^{-/-}$ MEFs with TCZ. At the end of the treatment, the live cells were simultaneously incubated with the $\Delta\Psi_m$ indicator TMRE and the plasma membrane integrity marker TOTO-3. As shown in Fig. 4B, D, J, and K, in response to TCZ, wild-type and FADD-reconstituted FADD$^{-/-}$ MEFs underwent $\Delta\Psi_m$ loss and were TOTO-3 positive. In contrast, FADD$^{-/-}$, RIP1$^{-/-}$, NEMO$^{-/-}$, and BAX$^{-/-}$ BAK$^{-/-}$ MEFs maintained $\Delta\Psi_m$ and were TOTO-3 negative (Fig. 4C, E, G, H, J, and K). Interestingly, although caspase 8$^{-/-}$ MEFs experienced significant $\Delta\Psi_m$ loss (Fig. 4F and J), plasma membrane integrity was intact, supporting results presented above that the lack of caspase 8 delays TCZ-induced $\Delta\Psi_m$ loss (Fig. 4F and K). Disruption of the necroptotic complex by necrostatin-1 in wild-type MEFs prevented $\Delta\Psi_m$ loss and preserved the plasma membrane integrity (Fig. 4I, J, and K). Furthermore, ablation of RIP3 using small interfering RNA (siRNA) in human endothelial cells attenuated the $\Delta\Psi_m$ loss triggered by TCZ treatment (Fig. 5A and B).

$\Delta\Psi_m$ is a determinant of cellular ATP levels and cell viability. Exposure to TCZ reduced ATP levels in wild-type cells (Fig. 6A and H), as well as in FADD$^{-/-}$ cells reexpressing FADD (Fig. 6C and H) but not in FADD$^{-/-}$ (Fig. 6B and H), RIP1$^{-/-}$ (Fig. 6D and H), NEMO$^{-/-}$ (Fig. 6F and H), and BAX$^{-/-}$ BAK$^{-/-}$ MEFs (Fig. 6G and H). Caspase 8$^{-/-}$ cells challenged with TCZ had a moderate reduction of ATP (Fig. 6E and H). Taken together, these data establish that RIP1-associated complex molecules play a crucial role in mitochondrial dysfunction. In addition, our findings consistently show the involvement of NEMO in TCZ-induced mitochondrial dysfunction.

NEMO but not RelA is required for TNF-α-induced necroptosis. The classical TNF-α-induced NF-κB activation pathway is dependent on NEMO and IKKβ (31). Our results indicate that NEMO$^{-/-}$ MEFs treated with TCZ failed to undergo bioenergetic collapse and cell death, indicating that NEMO

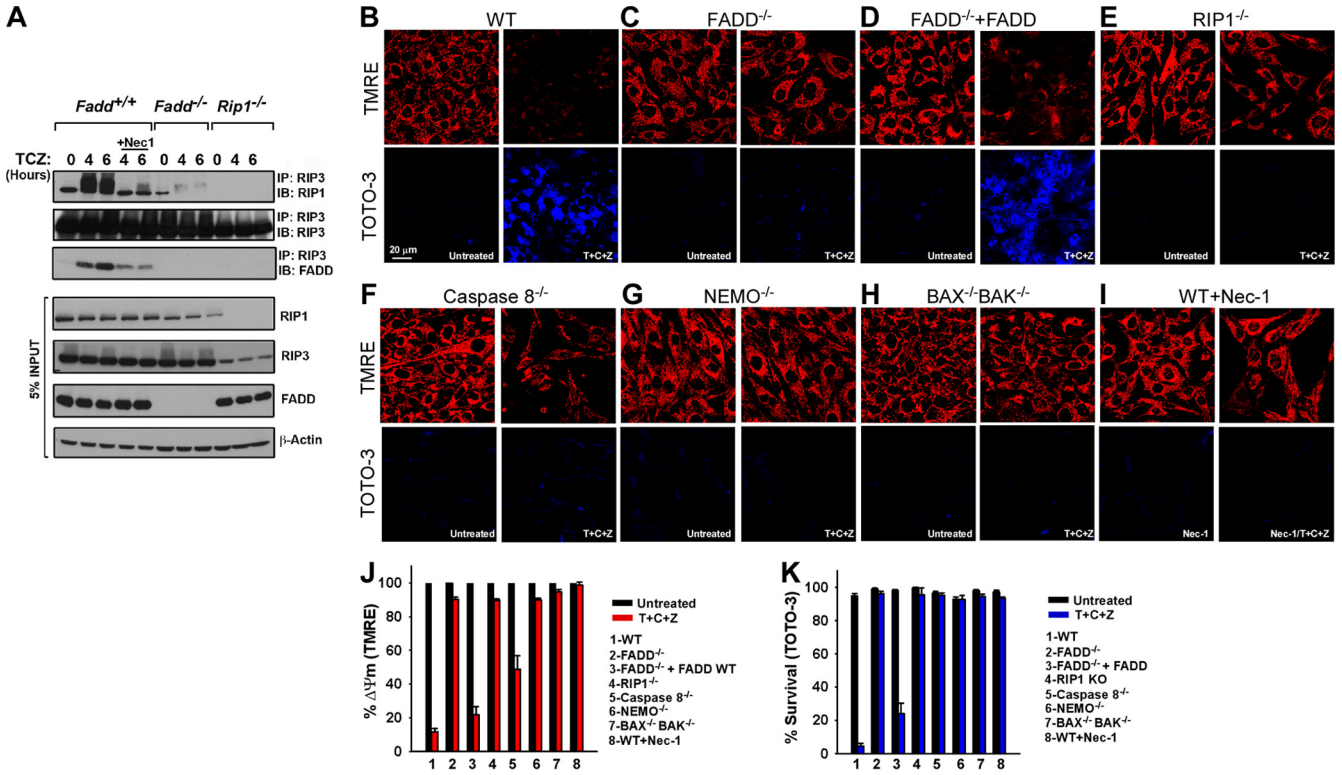

FIG. 4. FADD, RIP1, NEMO, and BAX/BAK determine the preservation of $\Delta\Psi_m$ and cell survival in TNF-α-induced necroptosis. (A) FADD is required for RIP1-RIP3 complex formation following TCZ challenge. WT, FADD$^{-/-}$, and RIP1$^{-/-}$ MEFs were treated as indicated, and equal amounts of cell lysates were used for coimmunoprecipitation (IP). The formation of FADD-RIP1-RIP3 complex is shown by RIP3 coimmunoprecipitation in wild-type, FADD$^{-/-}$, and RIP1$^{-/-}$ MEFs. Pellets from immunoprecipitation using an anti-RIP3 antibody were analyzed by Western blotting (immunoblotting [IB]) using anti-RIP1 and anti-FADD antibodies. Nec-1 (30 μM) pretreatment inhibits the TCZ-induced RIP1-RIP3 complex formation. MEFs were cultured in glass-bottom petri dishes, and cells were challenged with TCZ for 24 h. After the treatment, live cells were simultaneously loaded with mitochondrial membrane potential indicator TMRE (50 nM) and plasma membrane integrity marker TOTO-3 to assess mitochondrial function and cell viability, respectively. (B) Wild-type MEFs are positive for TOTO-3, and complete $\Delta\Psi_m$ loss was very significant. Conversely, FADD$^{-/-}$, RIP1$^{-/-}$, NEMO$^{-/-}$, and BAX$^{-/-}$ BAK$^{-/-}$ MEFs retained the $\Delta\Psi_m$ and cell viability (C, E, G, H, and K). (D) Reconstitution of full-length FADD in FADD$^{-/-}$ MEFs rescued the wild-type phenotype. (F) Caspase 8$^{-/-}$ MEFs experience a significant $\Delta\Psi_m$ loss but failed to undergo necroptotic cell death. (I) RIP1 inhibitor necrostatin-1 (30 μM) prevented the TCZ-induced $\Delta\Psi_m$ loss and cell death. (J and K) Quantitation of $\Delta\Psi_m$ maintenance and cell viability after TCZ treatment. The data in panels J and K are means ± SEMs of three or four independent experiments.

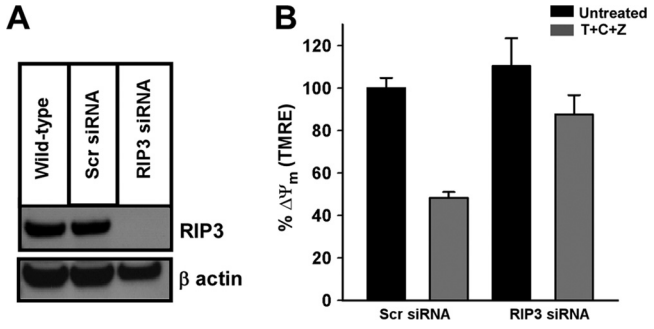

FIG. 5. Silencing of RIP3 attenuates TCZ-induced $\Delta\Psi_m$ loss. Human pulmonary endothelial cells transfected with a smart pool of human RIP3 siRNA were cultured for 48 h. (A) RIP3 protein levels after siRNA gene silencing at 48 h posttransfection in human pulmonary microvascular endothelial cells. (B) Cells were challenged with TCZ for 24 h and incubated with the $\Delta\Psi_m$ indicator TMRE for 20 min. $\Delta\Psi_m$ was measured using confocal microscopy. Data are presented as means ± SEMs of at least three independent experiments. Ser, scrambled.

and other NF-κB signaling components may have a role in necroptosis. Expression of human NEMO in NEMO$^{-/-}$ MEFs (Fig. 7A) completely rescued both TCZ-induced $\Delta\Psi_m$ loss (Fig. 7B and C) and cell death (Fig. 7D). NEMO binding to linear polyubiquitin chains in RIP1 is essential for NF-κB activation (58). Because NEMO$^{-/-}$ cells are insensitive to TCZ-induced necrosis and RIP1 undergoes RIP1-RIP3 complex formation during necroptosis, we speculated that the dependence on NEMO for necroptosis was due to a requirement of NEMO in TNF-α-induced FADD-RIP1-RIP3 complex formation. We next monitored whether NEMO is required for TNF-α-induced FADD-RIP1-RIP3 complex formation. Our biochemical analysis of necroptotic complex formation in wild-type and NEMO$^{-/-}$ cells indicated that NEMO is not involved in the FADD-RIP1-RIP3 interaction (Fig. 7E). To determine a possible involvement of IKKβ in necroptosis, wild-type MEFs were pretreated with a selective small-molecule IKKβ inhibitor, IMD-0354 (61). IMD-0354 (1 μM) preserved cellular ATP levels after challenge with TCZ (Fig. 7F). This result further supports the involvement of upstream NF-κB compo-

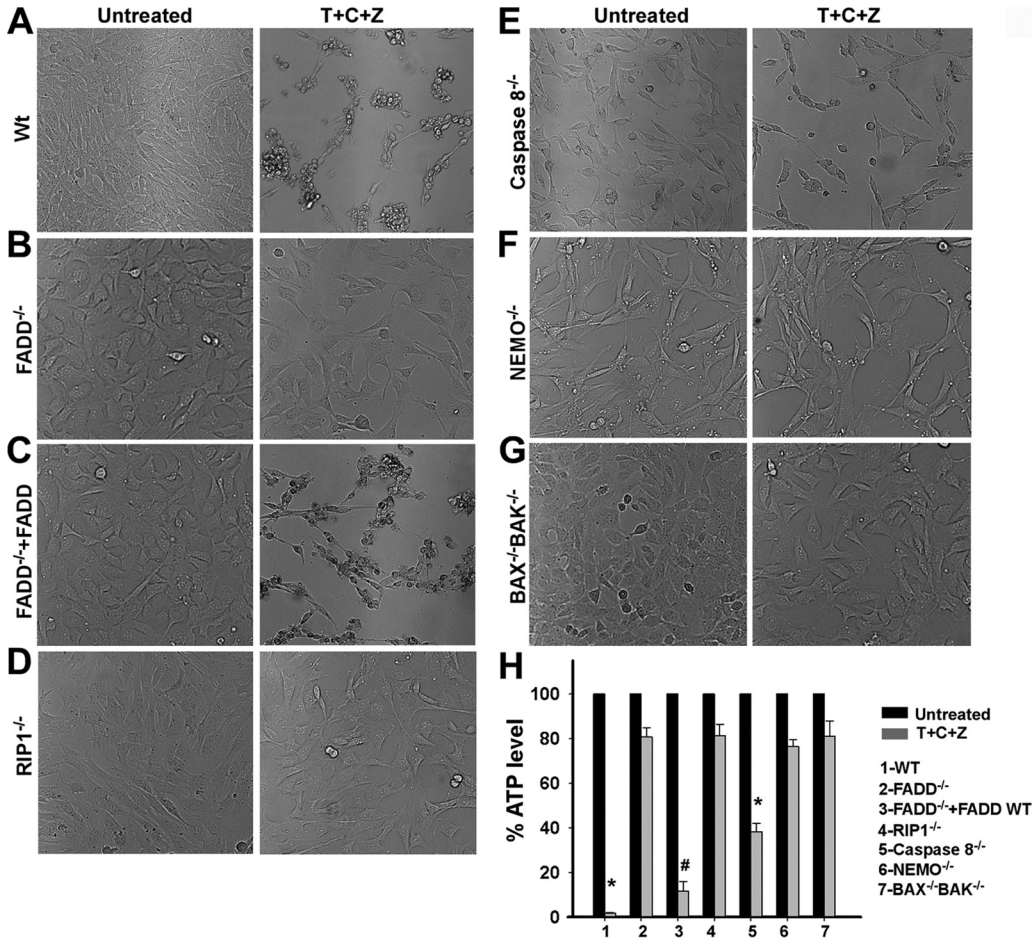

FIG. 6. TCZ-induced dissipation of ATP levels requires FADD, RIP1, NEMO, and BAX/BAK. Wild-type (A), FADD$^{-/-}$ (B), FADD$^{-/-}$ FADD (C), RIP1$^{-/-}$ (D), caspase 8$^{-/-}$ (E), NEMO$^{-/-}$ (F), and BAX$^{-/-}$ BAK$^{-/-}$ (G) MEFs were treated with TCZ for 20 h. (H) Cell viability was assessed by measuring ATP levels using a CellTiter-Glo luminescent cell viability assay kit. Data are presented as means ± SEMs of at least three independent experiments.

nents in TNF-α-induced necroptosis. In contrast, MEFs lacking RelA are susceptible to TCZ-induced cell death (Fig. 7G). There is a possibility that the phosphorylated IKKα-IKKβ-NEMO interaction might cause clustering and oligomerization with the RIP1-RIP3 complex which facilitate necroptosis. This hypothesis is supported by our observation that RelA KO cells are more sensitive to TCZ-induced cell death. Together, these results demonstrate that NEMO and IKKβ may have NF-κB-independent roles in TNF-α-induced necroptosis.

To continue investigation into the role of NEMO, we attempted to elucidate whether cytosolic exchange between FADD and NEMO$^{-/-}$ cells restores the TCZ effect. As shown in Fig. 8A, the TCZ-induced RIP1-RIP3 complex in the NEMO$^{-/-}$ cytosol fails to evoke $\Delta\Psi_m$ loss in the FADD$^{-/-}$ MEF mitochondrion-enriched pellet. Furthermore, we tested whether the components of the necroptotic complex bind to the mitochondria after treatment with TCZ. FADD was associated with the mitochondrial fraction (Fig. 8B) after 6 h of TCZ treatment (Fig. 8C). RIP3 binding was undetectable in the mitochondrial fraction after 4 and 6 h of TCZ treatment (data not shown). This approach indicated that the RIP1-RIP3 complex is insufficient for $\Delta\Psi_m$ loss by TCZ challenge. Together, these data suggest that NEMO may be required for functional activation of the necroptotic complex.

TNF-α-induced RIP1-RIP3 complex formation and mitochondrial dysfunction are Ca^{2+}-independent phenomena. Calcium participates in both short-term and long-term cell functions, including metabolism and gene transcription (5). Calcium signals are also crucial for both apoptosis and necrosis via mitochondrial depolarization (37). To determine the role of Ca^{2+} in TNF-α-induced necroptotic complex formation and mitochondrial dysfunction, wild-type MEFs were pretreated with the Ca^{2+} chelator 1,2-bis(*o*-aminophenoxy)ethane-*N*,*N*,*N*′,*N*′-tetraacetic acid tetra(acetoxymethyl) ester (BAPTA-AM) before TCZ challenge. BAPTA pretreatment did not affect the formation of the RIP1-RIP3 complex (Fig. 9A), $\Delta\Psi_m$ loss (Fig. 9B), or ATP depletion (Fig. 9C) induced by TCZ, indicating that cytosolic Ca^{2+} may not participate in the TCZ-induced necroptosis. The mitochondrial permeability transition pore has been implicated in several forms of cell death (22). Recent studies have demonstrated that the pore component cyclophilin D plays a critical role in necrotic cell death (1, 52, 59). To test whether cyclophilin D is involved in TCZ-induced $\Delta\Psi_m$

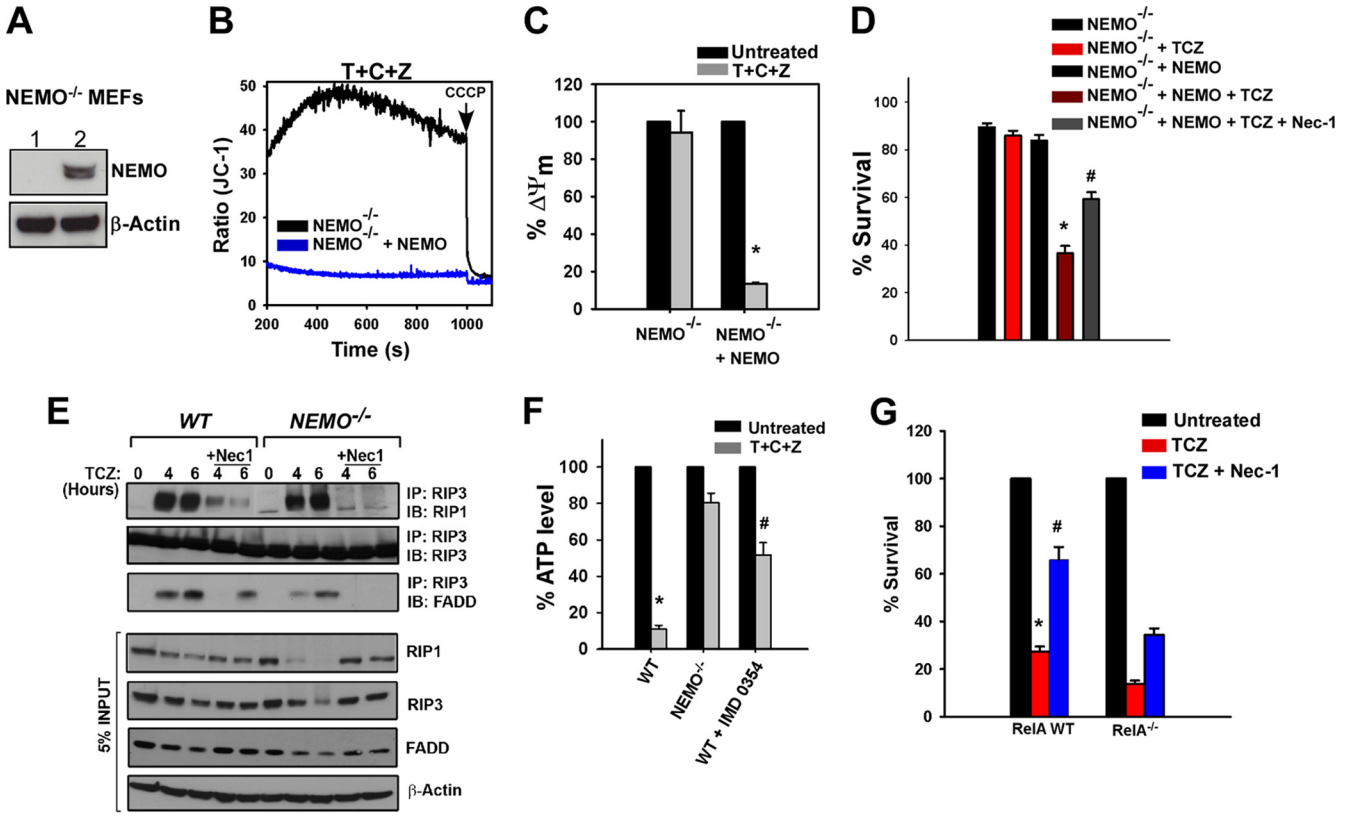

FIG. 7. NEMO but not RelA is required for the induction of TCZ-mediated necroptosis. (A) Expression of recombinant WT NEMO in NEMO-KO MEFs. $NEMO^{-/-}$ MEFs were transfected with human NEMO plasmid. Cell lysates were subjected to Western blotting and probed with anti-NEMO antibody. (B) MEFs were challenged for 20 h with TCZ or dimethyl sulfoxide. After the treatment, $NEMO^{-/-}$ MEFs and MEFs in which NEMO was reexpressed were permeabilized (40 μg/ml digitonin) and loaded with the ratiometric $\Delta\Psi_m$ fluorophore JC-1 and $\Delta\Psi_m$ was monitored. Cells were pulsed with the uncoupler carbonyl cyanide *m*-chlorophenylhydrazone (CCCP; 1 μM) at 1,000 s. (C) Quantitation of $\Delta\Psi_m$ maintenance in $NEMO^{-/-}$ MEFs and MEFs in which NEMO was reexpressed before and after TCZ treatment ($n = 3$; means ± SEMs). (D) Cell viability was determined at 24 h posttreatment. (E) Lack of NEMO does not alter the TCZ-induced FADD-RIP1-RIP3 complex formation. Wild-type and $NEMO^{-/-}$ MEFs were pretreated with Nec-1 (30 μM). These cells were then treated with TCZ and RIP3, and coimmunoprecipitation (IP) was performed. Immunoprecipitated eluates were subjected to immunoblotting (IB) for detection of the FADD-RIP1-RIP3 complex. (F) Wild-type MEFs were pretreated with selective IKKβ inhibitor IMD-0354 alone (1 μM; Tocris Bioscience, MO) or in combination with TCZ for 20 h. Cells were treated with dimethyl sulfoxide or IMD-0354 for 2 h prior to the TCZ challenge. ATP levels were determined by a CellTiter-Glo luminescent cell viability assay kit. Data are presented as means ± SEMs of at least quadruplicate experiments. (G) $RelA^{-/-}$ MEFs are susceptible to TCZ-induced cytotoxicity. $RelA^{+/+}$ and $RelA^{-/-}$ MEFs pretreated with or without Nec-1 (30 μM) were challenged with TCZ for 24 h, and cell viability was determined. Data are presented as means ± SEMs of at least three independent experiments.

loss, wild-type MEFs were pretreated with cyclosporine (2.5 μM) before TCZ challenge. Cyclosporine pretreatment did not prevent either TCZ-induced mitochondrial depolarization (Fig. 9D and E) or cell death (Fig. 9F). Together, these results indicate that both Ca^{2+} and cyclophilin D may not be involved in TCZ-induced cell death.

Bcl-x_L overexpression attenuates TNF-α-induced necroptosis. Prosurvival Bcl-2 proteins control many pathways of cell signaling, including programmed cell death in the mammalian system (71). Bcl-x_L prevents translocation of BAX to the mitochondria from the cytosol, oligomerization of BAX, and eventual outer mitochondrial membrane permeabilization (22). We tested the effect of Bcl-x_L on TNF-α-induced necroptosis. Overexpression of Bcl-x_L (Fig. 10A) attenuated TCZ-induced $\Delta\Psi_m$ loss and cell death (Fig. 10B and C). We next assessed whether BAX undergoes oligomerization after treatment with TCZ. TCZ treatment did not influence BAX oligomerization (Fig. 10D), indicating that BAX oligomerization may not participate in TCZ-induced necroptosis. Active forms of BH3-only proteins promote BAK and BAX activation, outer mitochondrial membrane permeabilization, and cytochrome *c* release (9). We analyzed cytochrome *c*, Smac/Diablo, HtraA2/Omi, and AIF release in TCZ-treated wild-type MEFs. Wild-type MEFs treated with TCZ induced partial cytochrome *c*, Smac/Diablo, and HtraA2/Omi release but not AIF release from the mitochondria (Fig. 10E and F), suggesting that mitochondrial permeabilization may be involved in TCZ-induced necroptosis.

Overexpression of mitochondrial and cytosolic antioxidants protects cells from necroptosis. NOX-family proteins and mitochondria are major sources of ROS. ROS regulate apoptosis and necrosis through oxidative modification, dysregulation of Ca^{2+} homeostasis, and opening of the mitochondrial permeability transition pore (34, 37). We tested whether induction of

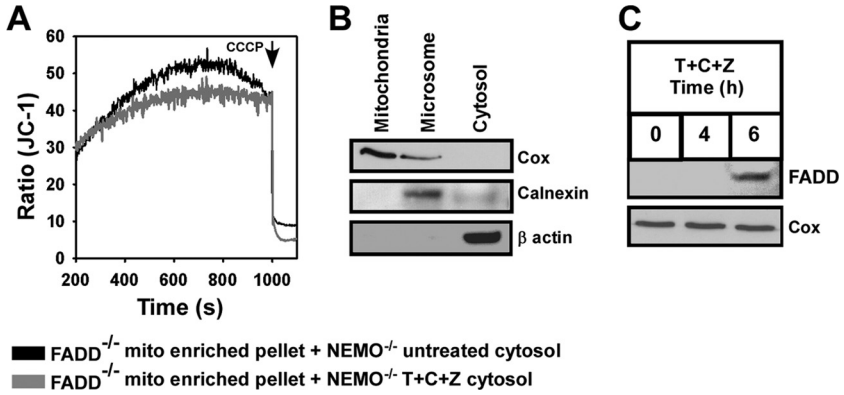

FIG. 8. RIP1-RIP3 complex-mediated $\Delta\Psi_m$ loss requires FADD and NEMO. FADD$^{-/-}$ and NEMO$^{-/-}$ MEFs were challenged for 20 h with TCZ or dimethyl sulfoxide. To perform cytosol exchange experiments, TCZ- or dimethyl sulfoxide-treated NEMO$^{-/-}$ MEFs were permeabilized for 6 min with intracellular medium containing digitonin (40 μg/ml). The cytosol was prepared after centrifugation at 20,000 rpm for 5 min. Similarly, an untreated FADD$^{-/-}$ MEF mitochondrion-enriched pellet was prepared for cytosol swap experiments. (A) TCZ-treated NEMO$^{-/-}$ MEF cytosol did not trigger $\Delta\Psi_m$ loss in FADD$^{-/-}$ MEF mitochondria. The arrow indicates the time at which FCCP was added. Data are presented as means ± SEMs of at least three independent experiments. TCZ induces association of FADD to mitochondria. CCCP, carbonyl cyanide *m*-chlorophenylhydrazone. (B) Subcellular fractionation of wild-type MEFs. Control and TCZ-treated wild-type MEFs were fractionated into mitochondrial, microsomal, and cytosolic fractions. The mitochondrial and microsomal fractions were lysed using radioimmunoprecipitation assay buffer, and the soluble proteins were analyzed for their purity. Subcellular fractions were immunoblotted with antibodies against cytochrome *c* oxidase (Cox), calnexin, and β-actin. (C) Purified mitochondria from both untreated and TCZ-treated MEFs (4 and 6 h) were lysed, and the supernatant was then analyzed by Western blotting with FADD, RIP3, and cytochrome *c* oxidase antibodies. Data are presented as means ± SEMs of at least three independent experiments.

TNF-α-induced necroptosis is associated with enhanced ROS production. Oxidation of the ROS indicator dichlorofluorescein (DCF) was elevated in wild-type cells following TCZ challenge (Fig. 11A and F). In sharp contrast, FADD$^{-/-}$ MEFs had no elevation of ROS after TCZ challenge (Fig. 11A). Reexpression of FADD in FADD$^{-/-}$ MEFs rescued the ROS burst (Fig. 11A). TCZ challenge also had no effect on ROS production in RIP1$^{-/-}$, caspase 8$^{-/-}$, and BAX$^{-/-}$ BAK$^{-/-}$ MEFs (Fig. 11B, C, E and F). Interestingly, NEMO$^{-/-}$ MEFs displayed enhancement of ROS levels after TCZ challenge (Fig. 11D). These results were confirmed by superoxide production in wild-type and knockout MEFs using DHE, a superoxide indicator (Fig. 11G). This result suggests that the source of ROS in NEMO$^{-/-}$ MEFs is most likely from mitochondria because MnSOD (encoded by *sod2*) is a TNF-α-inducible mitochondrial antioxidant enzyme that is transcriptionally regulated by NF-κB (18, 30). Since NEMO$^{-/-}$ MEFs have greatly reduced NF-κB activity following TNF-α challenge (48), it is likely that the level and activity of MnSOD are lower in NEMO$^{-/-}$ cells. Overexpression of either MnSOD or glutathione peroxidase 1 eliminated TCZ-induced ROS elevation and ATP reduction (Fig. 12B, C, E, and F), whereas the empty adenoviral vector alone afforded no protection (Fig. 12A, E, and F). The flavoprotein inhibitor diphenyleneiodonium (DPI) inhibits NOX enzyme activity. Cells treated with DPI displayed reduced ROS levels in response to TCZ challenge (Fig. 12D and E). ATP levels were not determined because DPI also inhibits mitochondrial flavoproteins that could alter mitochondrial function. Together, these results provide evidence that TNF-α induces appreciable ROS production during necroptosis and that elimination of this ROS production prevents ATP loss and cell death.

DISCUSSION

TNF-α is a pleiotropic cytokine that induces diverse biological responses ranging from inflammation to cell death. In most cells, TNF-α induces apoptosis, but under certain conditions it stimulates programmed necrosis (13, 66, 67). The mechanism by which the RIP1-RIP3 necroptotic complex triggers ATP loss has remained elusive since the discovery of TNF-α-mediated programmed necrosis. Here, we demonstrated that the TNF-α-dependent RIP1-RIP3 necroptotic complex alone is insufficient to elicit mitochondrial dysfunction, ATP loss, and programmed necrosis. TCZ-mediated necroptosis is dependent on the TNF-α signaling molecules FADD, RIP1, RIP3, and NEMO. This necroptotic complex leads to ROS production and mitochondrial dysfunction. This finding is important because mitochondria not only participate in apoptosis but also are involved in necroptosis. The recently described proinflammatory cytokine-induced necroptosis requires a unique RIP1-RIP3 pathway that impinges on cell function (10, 28, 72). The system described in our study might serve as a useful system for monitoring the translocation of a cytosolic factor(s) to the mitochondria that induces mitochondrial dysfunction during necroptosis.

Cells of the human Jurkat cell line lacking FADD undergo necroptosis via RIP1 and RIP3 by TNF-α (10). Primary T cells lacking either FADD or caspase 8 undergo autophagy, and RIP1 inhibition prevents cell death (4). Interestingly, necroptosis of FADD-deficient T cells failed to induce RIP1 cleavage or a RIP1-RIP3 complex formation (57). In contrast, MEFs lacking FADD are resistant to TNF-α-induced necrosis, and reconstitution of FADD restored both the apoptotic and necrotic phenotype induced by TNF-α (39). Here, we extend these studies to show that FADD is crucial for formation of the

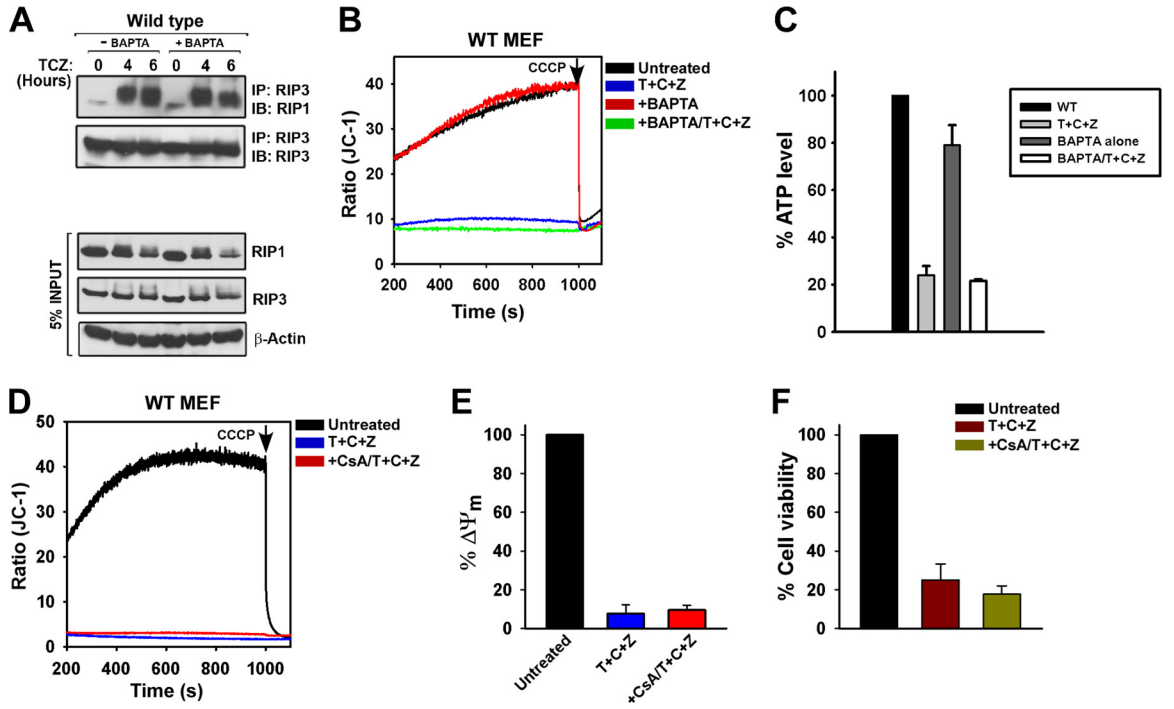

FIG. 9. Cytosolic calcium is dispensable for TCZ-induced RIP1-RIP3 complex formation and mitochondrial dysfunction during necroptosis. (A) Wild-type MEFs were challenged with TCZ in the absence or presence of BAPTA pretreatment. Cell lysates were subjected to immunoprecipitation (IP) with anti-RIP3 antibody. Immunoprecipitates were analyzed by Western blotting (immunoblotting [IB]) with anti-RIP1 antibody. (B) Chelation of cytosolic calcium did not prevent TCZ-induced $\Delta\Psi_m$ loss. Wild-type MEFs were treated with dimethyl sulfoxide or TCZ for 20 h. Permeabilized cells were loaded with the ratiometric mitochondrial membrane potential indicator JC-1, and $\Delta\Psi_m$ was examined. At 1,000 s, carbonyl cyanide *m*-chlorophenylhydrazone (CCCP) was added to dissipate the total $\Delta\Psi_m$. (C) MEFs were subjected to TCZ exposure following BAPTA pretreatment, and ATP levels were determined. (D) Wild-type MEFs were pretreated with cyclosporine (2.5 μM) before TCZ challenge. Permeabilized cells were loaded with JC-1, and $\Delta\Psi_m$ was measured. (E) Quantitation of $\Delta\Psi_m$ maintenance in wild-type MEFs with either TCZ alone or the combination of cyclosporine (CsA) and TCZ treatment. (F) Cell viability was determined at 24 h posttreatment. Data are presented as means ± SEMs of at least three independent experiments.

RIP1-RIP3 complex in fibroblasts. The bioenergetic parameters, including the mitochondrial respiration rate, $\Delta\Psi_m$, and ATP levels, are preserved in TCZ-challenged FADD$^{-/-}$ MEFs (Fig. 1, 2, 4, and 7). RIP-family proteins play important roles in both cell survival and cell death (50). However, genetic ablation of RIP3 in mice had no physiological phenotype (54), but deletion of RIP1 caused severe death in lymphoid and adipose tissue and mice exhibited postnatal lethality (32). RIP1 but not RIP3 is indispensable for NF-κB activation in response to TNF-α (10, 28, 32). Genetic ablation of TNF-α signaling downstream candidates RIP1$^{-/-}$ (RIP KO) and RIP3 (siRNA-mediated knockdown) prevents the TCZ-induced mitochondrial dysfunction (Fig. 1, 2, 4, 5, and 6), indicating the contribution of the RIP1-RIP3 complex in mitochondrion-dependent necroptosis. In addition, cytosol exchange experiments also demonstrate that RIP1 is essential for $\Delta\Psi_m$ loss (Fig. 2). TNF-α-induced RIP1-FADD-caspase 8 complex formation and the following recruitment of RIP3 exquisitely potentiate necroptotic cell death, while disruption of this complex by necrostatin-1 effectively inhibits necroptosis (28). Consistent with previous findings, prevention of the necroptotic complex by the RIP1 inhibitor Nec-1 inhibits $\Delta\Psi_m$ loss and cell death (Fig. 4A, I, J, and K). TNF-α-induced caspase 8 activation results in RIP1 cleavage and halts the necrotic cell death but facilitates apoptosis (40). Our study suggests that cells lacking caspase 8 undergo a delayed $\Delta\Psi_m$ loss in a permeabilized system and considerable loss of $\Delta\Psi_m$ and ATP levels in an intact system after TCZ treatment (Fig. 2, 3, 4, and 6). Though TCZ-induced dissipation of $\Delta\Psi_m$ and ATP levels occurs in caspase 8$^{-/-}$ MEFs, the plasma membrane integrity failed to deteriorate, suggesting that the NEMO-FADD-RIP1-RIP3 complex could still cause bioenergetic collapse (Fig. 4 and 6). TNF-α–CHX-induced apoptosis is defective in caspase 8$^{-/-}$ MEFs (data not shown). It is possible that the absence of caspase 8 could delay the plasma membrane permeability in necroptosis (Fig. 4F, J, and K). On the basis of less ROS burst in caspase 8$^{-/-}$ MEFs, we speculate that ROS-mediated lipid peroxidation may contribute to plasma membrane integrity loss in necroptosis.

TNF-α-induced NF-κB activation requires NEMO, IKKβ-dependent IκB phosphorylation and degradation and dissociation of cytosolic NF-κB to form a heterodimer. Cells lacking NEMO still maintain modest NF-κB2 activity via a noncanonical pathway that requires IKKα and NF-κB-inducing kinase (NIK) for cell survival (11). The results presented here indicate that cells lacking NEMO are insensitive to TCZ challenge and that the mitochondrial bioenergetics remain intact (Fig. 1, 2, 3, 4, and 6). Further, pharmacologic blockage of NF-κB with an IKKβ inhibitor prevented the reduction of ATP levels by necroptosis (Fig. 7F). Although the involvement of IκBα kinases in TNF-α-induced necroptosis is an interesting area to be

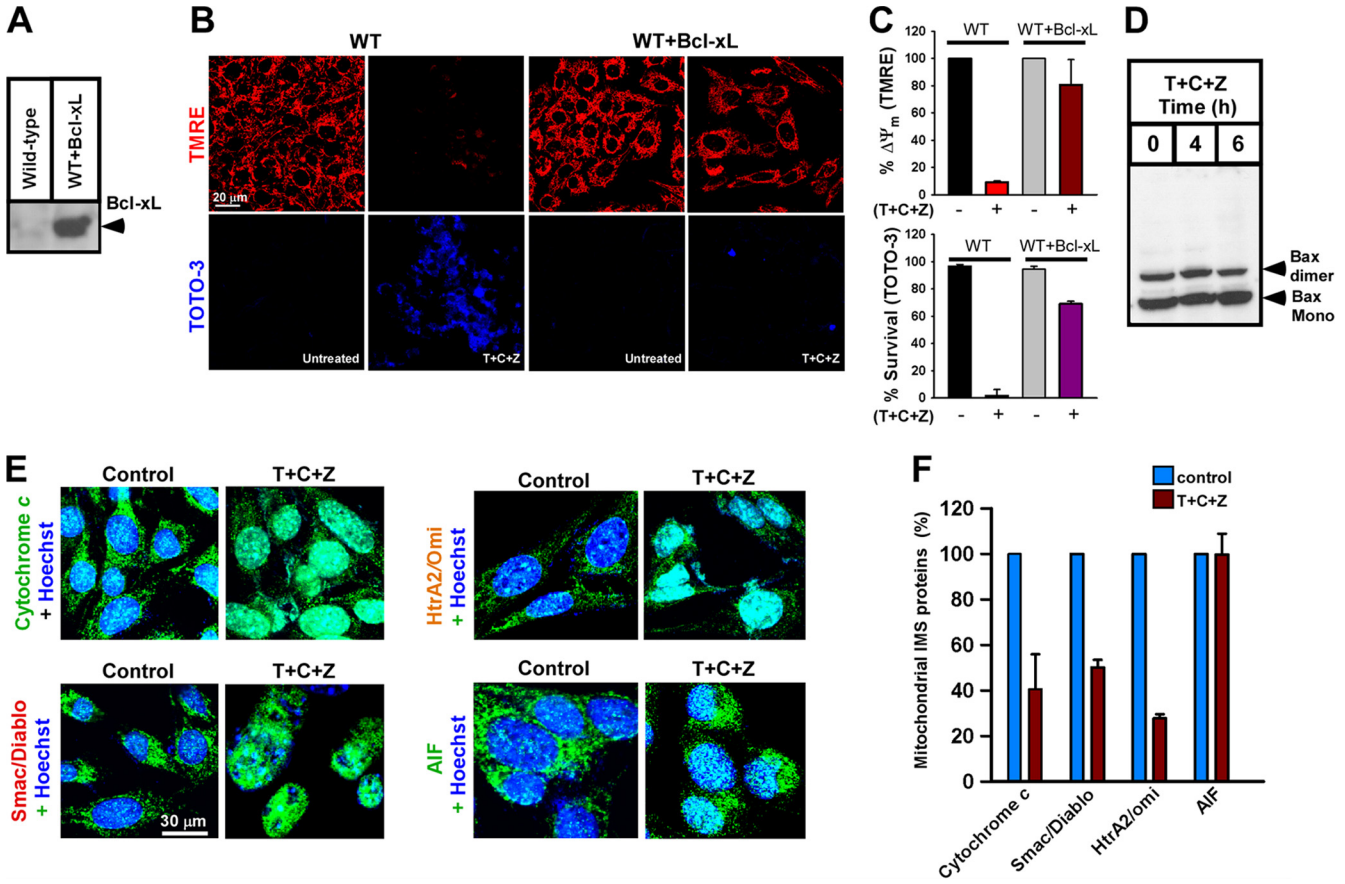

FIG. 10. Overexpression of Bcl-x_L attenuates TCZ-induced necroptosis. (A) Wild-type MEFs were transfected with Bcl-x_L plasmid. The overexpression of Bcl-x_L was assessed by Western blotting. (B) MEFs were cultured in glass-bottom petri dishes, and cells were challenged with TCZ for 20 h. After the treatment, live cells were simultaneously loaded with the $\Delta\Psi_m$ indicator TMRE and the plasma membrane integrity marker TOTO-3 to assess the mitochondrial function and cell viability, respectively. (C) Quantitation of $\Delta\Psi_m$ maintenance and cell viability after TCZ treatment. (D) Wild-type MEFs were treated with TCZ for 4 and 6 h. Cells were isolated and treated with 10 mM bis-maleimide cross-linker. The BAX oligomers were analyzed by anti-BAX immunoblotting. (E) Wild-type MEFs were treated with TCZ for 6 h, and cells were fixed and immunostained with anti-cytochrome *c* antibody (green), anti-Smac/Diablo antibody (green), anti-HtrA2/Omi (green), and anti-AIF antibody (green). Hoechst dye (blue) was used as a nuclear stain. (F) Quantitation of mitochondrial intermembrane space proteins (cytochrome *c*, Smac/Diablo, HtrA2/Omi, and AIF). Data are presented as means ± SEMs of at least three independent experiments.

investigated, our findings suggest that upstream NF-κB molecules IKKβ and NEMO but not RelA likely participate in TNF-α-induced mitochondrial dysfunction.

The mitochondrion is an organelle with two well-defined compartments, the matrix and the intermembrane space, which are bounded by the inner mitochondrial membrane (IMM) and the outer mitochondrial membrane (OMM), respectively. In order to maintain the function and metabolism of the mitochondria, the inner membrane is highly selective and permeable to limited ions and metabolites. The highly selective nature of the inner membrane allows the establishment of a proton-motive electrochemical force across the mitochondrial inner membrane, which can be converted by F_0F_1 ATP synthase into ATP. Mitochondrial PTP opening consists of a voltage-dependent anion channel, cyclophilin D, and adenine nucleotide translocase (ANT) and is implicated in necrosis (1, 62). However, disagreement continues as to the role of the voltage-dependent anion channel (VDAC) in PTP opening (2). Furthermore, studies demonstrated that mice lacking the Ppif gene (cyclophilin D) are resistant to Ca^{2+}-dependent PTP opening (1, 3, 24, 52). The most abundant mitochondrial ANT has two states, the cytosolic state (c state) and the matrix state (m state) (62). It plays a vital role in ATP flux from mitochondria. However, ANT can switch to a lethal function corresponding to its pore-forming activity. Direct application of zVAD in a permeabilized system did not induce PTP opening or $\Delta\Psi_m$ loss in either control ot TNF-α-stimulated cells. In contrast, ANT inhibitor atractyloside induced a rapid mitochondrial membrane depolarization (data not shown). These results indicate that zVAD may not have a direct effect on the mitochondria. We postulate that manipulation of the ANT isoforms with zVAD has little or no impact on the mitochondrial membrane potential. On the other hand, mitochondrial outer membrane permeabilization plays a crucial role in apoptosis that is regulated via Bcl-2-family proteins (23, 33, 53, 55). The interaction of proapoptotic effector Bcl-2 members BAK and BAX with cytosolic BH3-only proteins facilitates oligomerization, which leads to OMM permeabilization (35, 47). Cells lacking both BAK and BAX are insensitive to apoptosis (7, 41). The loss of ATP is remarkable in TNF-α-induced

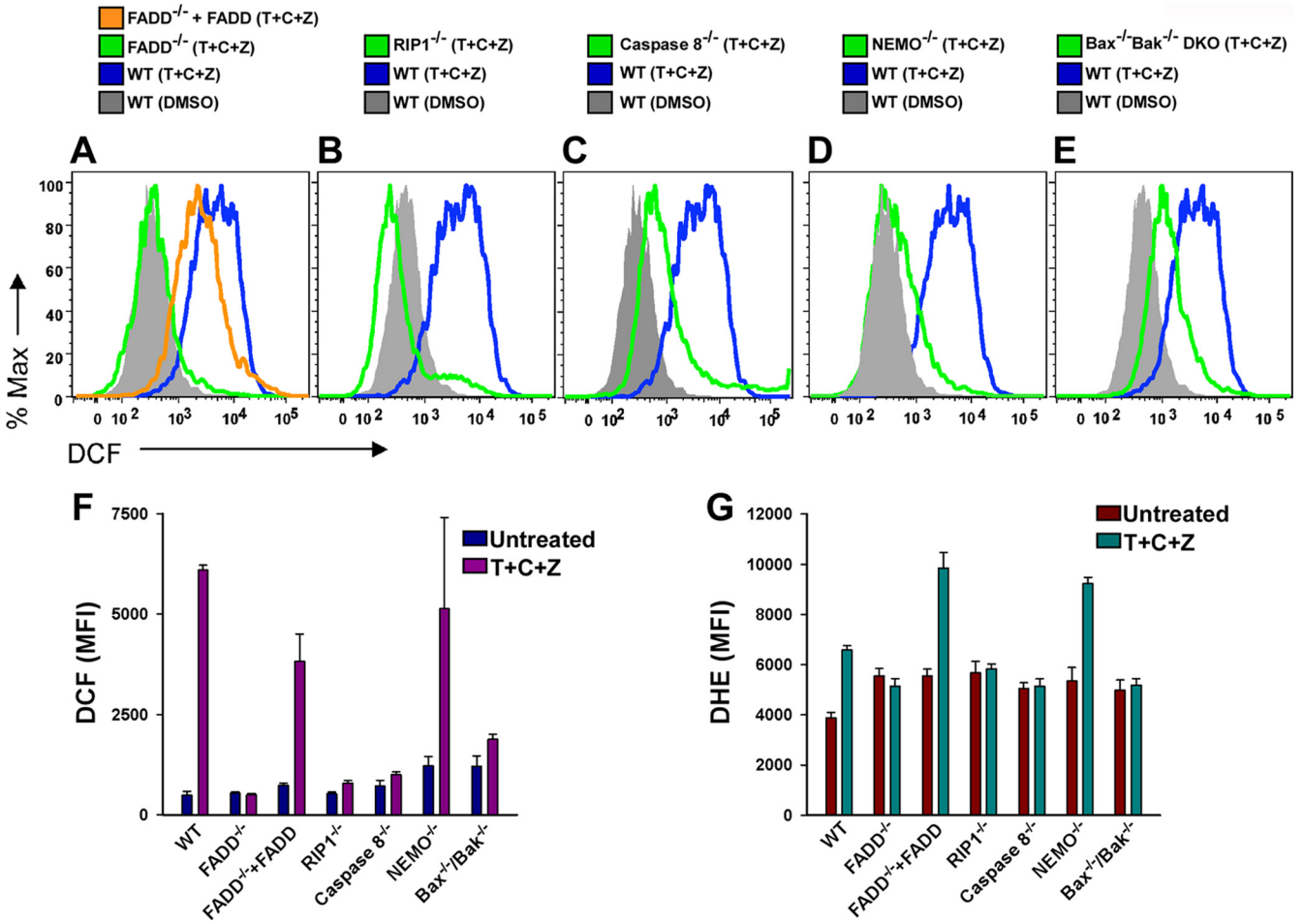

FIG. 11. TCZ-induced reactive oxygen species production is FADD and RIP1 dependent. MEFs were treated with dimethyl sulfoxide (DMSO) or TCZ for 12 h. Cells were then loaded with ROS indicator dichlorofluorescein diacetate (H_2DCF-DA; 10 μM), and fluorescence intensity was assessed by flow cytometry. (A) Wild-type MEFs challenged with TCZ exhibited a large rise in ROS levels, whereas FADD$^{-/-}$ cells failed to increase ROS production. Stable reexpression of full-length FADD in FADD$^{-/-}$ cells reestablished the ROS elevation after TCZ challenge. RIP1$^{-/-}$ (B), caspase 8$^{-/-}$ (C), and BAX$^{-/-}$ BAK$^{-/-}$ (E) cells produced nominal ROS. (D) NEMO$^{-/-}$ MEFs challenged with TCZ displayed ROS elevation. (F) Quantitation of DCF fluorescence change after TCZ treatment. (G) Quantitation of DHE fluorescence after TCZ treatment. Data are presented as means ± SEMs of at least three independent experiments.

necroptosis, but the induction of mitochondrial malfunction is unknown. Surprisingly, MEFs deficient in both BAX and BAK failed to undergo necroptosis in response to TCZ (Fig. 4). In addition, our cytosol swap approach further confirmed that BAX/BAK is necessary for mitochondrion-dependent downstream necroptotic signaling. Though it is uncertain how BAX and BAK control necroptotic complex-induced mitochondrial malfunction at the subcellular milieu, interestingly, upstream FADD-RIP1-RIP3 necroptotic complex formation was not disrupted in BAX/BAK-DKO MEFs (Fig. 3). Because necroptotic complex formation remains unaffected, in BAX/BAK-DKO MEFs, it is possible that the necroptotic complex could interact with BAK to initiate mitochondrial membrane depolarization that leads to bioenergetic collapse.

Though mitochondria are biological engines for a multitude of functions such as nutrient oxidation, ATP production, Ca^{2+} buffering, and ROS production, the mitochondrial dysfunction in pathological settings could be caused by Ca^{2+} overload, permeability transition pore opening, and overproduction of ROS (56). Robust ROS production has been implicated in TNF-α-induced necrosis through either members of the NOX family or mitochondria (34). Disruption of the mitochondrial respiration rate induces proton gradient collapse and electron leakage from the mitochondrial matrix and favors ROS production. In the context of TCZ-induced necroptosis, ROS levels are elevated in wild-type cells but not in FADD-, RIP1-, caspase 8-, and BAX/BAK-deficient cells, which suggests that both NOX-family- and mitochondrion-dependent pathways are involved in ROS production (Fig. 11 and 12). Mitochondrial and cytosolic antioxidants are the target of NF-κB at the transcription level (30). Interestingly, NEMO$^{-/-}$ MEFs did not prevent the TCZ-induced overproduction of ROS. Cells lacking p65 show lower levels of antioxidant transcripts following TNF-α stimulation (unpublished data). It is conceivable that an imbalance of oxidant/antioxidant levels occurs in NF-κB-deficient cells following TNF-α stimulation. siRNA knockdown of NOXO1 or pretreatment with ROS scavengers attenuates the TNF-α-induced RIP1-dependent ROS elevation and

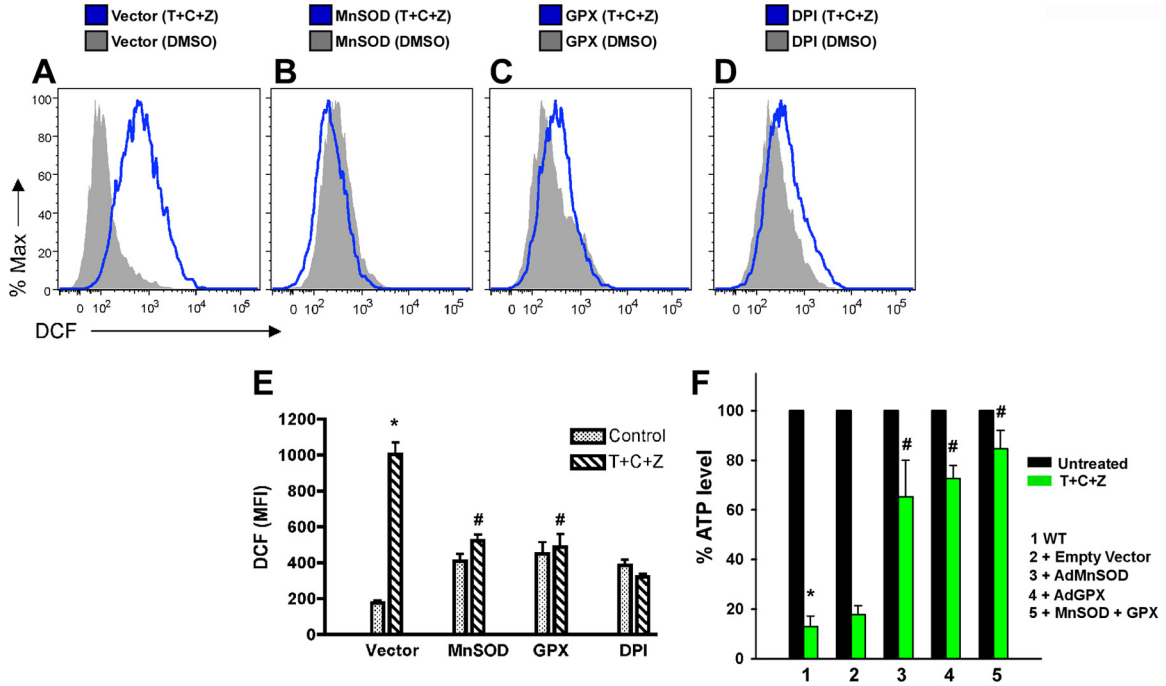

FIG. 12. Overexpression of cytosolic and mitochondrial antioxidants alleviates the TCZ-induced ROS production. Wild-type MEFs were transduced with empty adenoviral vector (Ad5CMV), MnSOD, or GPX for 36 h. Transduced cells were treated with TCZ for 14 h. Wild-type cells were treated with TCZ for 12 h and the flavoprotein inhibitor DPI (20 μM) for 2 h. Cells were loaded with CMH_2DCF-DA, and ROS levels were assessed by flow cytometry. (A) Cells transduced with the empty vector alone challenged with TCZ demonstrated an increase ROS production. MnSOD (B) or glutathione peroxidase (C) overexpression attenuated the TCZ-induced ROS production. (D) Similarly, DPI supplementation prevented the ROS elevation. (E) Quantitation of ROS levels in MnSOD, glutathione peroxidase-overexpressed, or DPI-treated TCZ samples. Data are presented as means ± SEMs of at least triplicate experiments. (F) Wild-type MEFs were overexpressed with adenoviral empty vector, MnSOD, GPX, or the combination of MnSOD and glutathione peroxidase. MEFs were subjected to TCZ exposure, and ATP levels were determined by a CellTiter-Glo luminescent cell viability assay kit. Data are presented as means ± SEMs of at least three independent experiments.

subsequently improves cell survival (34). Using pharmacologic and genetic approaches, we have now demonstrated that TCZ-induced ROS play a crucial role in mitochondrial dysfunction and that overexpression of mitochondrion-targeted and cytosolic antioxidants or inhibition of ROS production preserves the ATP levels (Fig. 12). Similar to apoptosis, prevention of necroptosis-induced mitochondrial damage might improve the management of organ function.

More generally, the results presented here provide further understanding of the role of mitochondria in inflammation-induced necroptosis. Using multiple TNF-α signaling molecule-knockout cells, our mitochondrial functional studies provide evidence that mitochondria play an amplifying role in the pathophysiology of inflammation-induced necroptosis.

ACKNOWLEDGMENTS

We thank Astar Winoto, Michael Karin, and Michelle Kelliher for providing the FADD-, NEMO-, and RIP1-KO MEFs, respectively. We acknowledge Suresh K. Joseph and Wei-Xing Zong for providing calnexin antibody and the Bcl-x_L plasmid construct, respectively. We thank Kevin J. Foskett, Craig B. Thompson, Richard N. Kitsis, and Jonathan Soboloff for critically reading the manuscript, helpful thoughts, and suggestions. We are also thankful to Håkan Steen for assistance with ATP assays and helpful discussions.

This work was supported by National Institutes of Health grants (R01 HL086699, HL086699-01A2S1, 1S10RR027327-01) to M.M. and an ACS research scholar grant (RSG-09-195-01-MPC) to S.B.

REFERENCES

1. **Baines, C. P., et al.** 2005. Loss of cyclophilin D reveals a critical role for mitochondrial permeability transition in cell death. Nature **434:**658–662.
2. **Baines, C. P., R. A. Kaiser, T. Sheiko, W. J. Craigen, and J. D. Molkentin.** 2007. Voltage-dependent anion channels are dispensable for mitochondrial-dependent cell death. Nat. Cell Biol. **9:**550–555.
3. **Basso, E., et al.** 2005. Properties of the permeability transition pore in mitochondria devoid of cyclophilin D. J. Biol. Chem. **280:**18558–18561.
4. **Bell, B. D., et al.** 2008. FADD and caspase-8 control the outcome of autophagic signaling in proliferating T cells. Proc. Natl. Acad. Sci. U. S. A. **105:**16677–16682.
5. **Berridge, M. J., M. D. Bootman, and H. L. Roderick.** 2003. Calcium signalling: dynamics, homeostasis and remodelling. Nat. Rev. Mol. Cell Biol. **4:**517–529.
6. **Boldin, M. P., T. M. Goncharov, Y. V. Goltsev, and D. Wallach.** 1996. Involvement of MACH, a novel MORT1/FADD-interacting protease, in Fas/APO-1- and TNF receptor-induced cell death. Cell **85:**803–815.
7. **Brunelle, J. K., and A. Letai.** 2009. Control of mitochondrial apoptosis by the Bcl-2 family. J. Cell Sci. **122:**437–441.
8. **Burwell, L. S., and P. S. Brookes.** 2008. Mitochondria as a target for the cardioprotective effects of nitric oxide in ischemia-reperfusion injury. Antioxid. Redox Signal. **10:**579–599.
9. **Chipuk, J. E., T. Moldoveanu, F. Llambi, M. J. Parsons, and D. R. Green.** 2010. The BCL-2 family reunion. Mol. Cell **37:**299–310.
10. **Cho, Y. S., et al.** 2009. Phosphorylation-driven assembly of the RIP1-RIP3 complex regulates programmed necrosis and virus-induced inflammation. Cell **137:**1112–1123.
11. **Claudio, E., K. Brown, S. Park, H. Wang, and U. Siebenlist.** 2002. BAFF-induced NEMO-independent processing of NF-kappa B2 in maturing B cells. Nat. Immunol. **3:**958–965.
12. **Cleveland, J. L., and J. N. Ihle.** 1995. Contenders in FasL/TNF death signaling. Cell **81:**479–482.
13. **Das, M., et al.** 2009. Induction of hepatitis by JNK-mediated expression of TNF-alpha. Cell **136:**249–260.
14. **Davis, C. W., et al.** 2010. Nitration of the mitochondrial complex I subunit

NDUFB8 elicits RIP1- and RIP3-mediated necrosis. Free Radic. Biol. Med. **48:**306–317.
15. **Degterev, A., et al.** 2008. Identification of RIP1 kinase as a specific cellular target of necrostatins. Nat. Chem. Biol. **4:**313–321.
16. **Degterev, A., et al.** 2005. Chemical inhibitor of nonapoptotic cell death with therapeutic potential for ischemic brain injury. Nat. Chem. Biol. **1:**112–119.
17. **Degterev, A., and J. Yuan.** 2008. Expansion and evolution of cell death programmes. Nat. Rev. Mol. Cell Biol. **9:**378–390.
18. **Dhar, S. K., Y. Xu, and D. K. St. Clair.** 2010. Nuclear factor kappaB- and specificity protein 1-dependent p53-mediated bi-directional regulation of the human manganese superoxide dismutase gene. J. Biol. Chem. **285:**9835–9846.
19. **Droge, W.** 2002. Free radicals in the physiological control of cell function. Physiol. Rev. **82:**47–95.
20. **Galluzzi, L., and G. Kroemer.** 2008. Necroptosis: a specialized pathway of programmed necrosis. Cell **135:**1161–1163.
21. **Ghosh, S., and M. S. Hayden.** 2008. New regulators of NF-kappaB in inflammation. Nat. Rev. Immunol. **8:**837–848.
22. **Green, D. R., and G. Kroemer.** 2004. The pathophysiology of mitochondrial cell death. Science **305:**626–629.
23. **Gross, A., J. M. McDonnell, and S. J. Korsmeyer.** 1999. BCL-2 family members and the mitochondria in apoptosis. Genes Dev. **13:**1899–1911.
24. **Halestrap, A. P.** 2006. Calcium, mitochondria and reperfusion injury: a pore way to die. Biochem. Soc. Trans. **34:**232–237.
25. **Hamanaka, R. B., and N. S. Chandel.** 2010. Mitochondrial reactive oxygen species regulate cellular signaling and dictate biological outcomes. Trends Biochem. Sci. **35:**505–513.
26. **Hawkins, B. J., et al.** 2010. S-glutathionylation activates STIM1 and alters mitochondrial homeostasis. J. Cell Biol. **190:**391–405.
27. **Hawkins, B. J., et al.** 2007. G protein-coupled receptor Ca^{2+}-linked mitochondrial reactive oxygen species are essential for endothelial/leukocyte adherence. Mol. Cell. Biol. **27:**7582–7593.
28. **He, S., et al.** 2009. Receptor interacting protein kinase-3 determines cellular necrotic response to TNF-alpha. Cell **137:**1100–1111.
29. **Hitomi, J., et al.** 2008. Identification of a molecular signaling network that regulates a cellular necrotic cell death pathway. Cell **135:**1311–1323.
30. **Jones, P. L., D. Ping, and J. M. Boss.** 1997. Tumor necrosis factor alpha and interleukin-1beta regulate the murine manganese superoxide dismutase gene through a complex intronic enhancer involving C/EBP-beta and NF-kappaB. Mol. Cell. Biol. **17:**6970–6981.
31. **Karin, M., and F. R. Greten.** 2005. NF-kappaB: linking inflammation and immunity to cancer development and progression. Nat. Rev. Immunol. **5:**749–759.
32. **Kelliher, M. A., et al.** 1998. The death domain kinase RIP mediates the TNF-induced NF-kappaB signal. Immunity **8:**297–303.
33. **Kim, H., et al.** 2009. Stepwise activation of BAX and BAK by tBID, BIM, and PUMA initiates mitochondrial apoptosis. Mol. Cell **36:**487–499.
34. **Kim, Y. S., M. J. Morgan, S. Choksi, and Z. G. Liu.** 2007. TNF-induced activation of the Nox1 NADPH oxidase and its role in the induction of necrotic cell death. Mol. Cell **26:**675–687.
35. **Kuwana, T., et al.** 2002. Bid, Bax, and lipids cooperate to form supramolecular openings in the outer mitochondrial membrane. Cell **111:**331–342.
36. **Lambeth, J. D.** 2004. NOX enzymes and the biology of reactive oxygen. Nat. Rev. Immunol. **4:**181–189.
37. **Lemasters, J. J., T. P. Theruvath, Z. Zhong, and A. L. Nieminen.** 2009. Mitochondrial calcium and the permeability transition in cell death. Biochim. Biophys. Acta **1787:**1395–1401.
38. **Li, H., H. Zhu, C. J. Xu, and J. Yuan.** 1998. Cleavage of BID by caspase 8 mediates the mitochondrial damage in the Fas pathway of apoptosis. Cell **94:**491–501.
39. **Lin, Y., et al.** 2004. Tumor necrosis factor-induced nonapoptotic cell death requires receptor-interacting protein-mediated cellular reactive oxygen species accumulation. J. Biol. Chem. **279:**10822–10828.
40. **Lin, Y., A. Devin, Y. Rodriguez, and Z. G. Liu.** 1999. Cleavage of the death domain kinase RIP by caspase-8 prompts TNF-induced apoptosis. Genes Dev. **13:**2514–2526.
41. **Lindsten, T., et al.** 2000. The combined functions of proapoptotic Bcl-2 family members bak and bax are essential for normal development of multiple tissues. Mol. Cell **6:**1389–1399.
42. **Luo, X., I. Budihardjo, H. Zou, C. Slaughter, and X. Wang.** 1998. Bid, a Bcl2 interacting protein, mediates cytochrome c release from mitochondria in response to activation of cell surface death receptors. Cell **94:**481–490.
43. **Madesh, M., B. Antonsson, S. M. Srinivasula, E. S. Alnemri, and G. Hajnoczky.** 2002. Rapid kinetics of tBid-induced cytochrome c and Smac/DIABLO release and mitochondrial depolarization. J. Biol. Chem. **277:**5651–5659.
44. **Madesh, M., and G. Hajnoczky.** 2001. VDAC-dependent permeabilization of the outer mitochondrial membrane by superoxide induces rapid and massive cytochrome c release. J. Cell Biol. **155:**1003–1015.
45. **Madesh, M., et al.** 2005. Selective role for superoxide in InsP3 receptor-mediated mitochondrial dysfunction and endothelial apoptosis. J. Cell Biol. **170:**1079–1090.
46. **Madesh, M., S. A. Ibrahim, and K. A. Balasubramanian.** 1997. Phospholipase D activity in the intestinal mitochondria: activation by oxygen free radicals. Free Radic. Biol. Med. **23:**271–277.
47. **Madesh, M., et al.** 2009. Execution of superoxide-induced cell death by the proapoptotic Bcl-2-related proteins Bid and Bak. Mol. Cell. Biol. **29:**3099–3112.
48. **Makris, C., et al.** 2000. Female mice heterozygous for IKK gamma/NEMO deficiencies develop a dermatopathy similar to the human X-linked disorder incontinentia pigmenti. Mol. Cell **5:**969–979.
49. **Mangan, D. F., G. R. Welch, and S. M. Wahl.** 1991. Lipopolysaccharide, tumor necrosis factor-alpha, and IL-1 beta prevent programmed cell death (apoptosis) in human peripheral blood monocytes. J. Immunol. **146:**1541–1546.
50. **Meylan, E., and J. Tschopp.** 2005. The RIP kinases: crucial integrators of cellular stress. Trends Biochem. Sci. **30:**151–159.
51. **Muzio, M., et al.** 1996. FLICE, a novel FADD-homologous ICE/CED-3-like protease, is recruited to the CD95 (Fas/APO-1) death-inducing signaling complex. Cell **85:**817–827.
52. **Nakagawa, T., et al.** 2005. Cyclophilin D-dependent mitochondrial permeability transition regulates some necrotic but not apoptotic cell death. Nature **434:**652–658.
53. **Newmeyer, D. D., and S. Ferguson-Miller.** 2003. Mitochondria: releasing power for life and unleashing the machineries of death. Cell **112:**481–490.
54. **Newton, K., X. Sun, and V. M. Dixit.** 2004. Kinase RIP3 is dispensable for normal NF-kappa Bs, signaling by the B-cell and T-cell receptors, tumor necrosis factor receptor 1, and Toll-like receptors 2 and 4. Mol. Cell. Biol. **24:**1464–1469.
55. **Ni, H. M., et al.** 2010. Bid agonist regulates murine hepatocyte proliferation by controlling endoplasmic reticulum calcium homeostasis. Hepatology **52:**338–348.
56. **Orrenius, S., B. Zhivotovsky, and P. Nicotera.** 2003. Regulation of cell death: the calcium-apoptosis link. Nat. Rev. Mol. Cell Biol. **4:**552–565.
57. **Osborn, S. L., et al.** 2010. Fas-associated death domain (FADD) is a negative regulator of T-cell receptor-mediated necroptosis. Proc. Natl. Acad. Sci. U. S. A. **107:**13034–13039.
58. **Rahighi, S., et al.** 2009. Specific recognition of linear ubiquitin chains by NEMO is important for NF-kappaB activation. Cell **136:**1098–1109.
59. **Schinzel, A. C., et al.** 2005. Cyclophilin D is a component of mitochondrial permeability transition and mediates neuronal cell death after focal cerebral ischemia. Proc. Natl. Acad. Sci. U. S. A. **102:**12005–12010.
60. **Scorrano, L., et al.** 2003. BAX and BAK regulation of endoplasmic reticulum Ca^{2+}: a control point for apoptosis. Science **300:**135–139.
61. **Tanaka, A., et al.** 2005. A novel NF-kappaB inhibitor, IMD-0354, suppresses neoplastic proliferation of human mast cells with constitutively activated c-kit receptors. Blood **105:**2324–2331.
62. **Temkin, V., Q. Huang, H. Liu, H. Osada, and R. M. Pope.** 2006. Inhibition of ADP/ATP exchange in receptor-interacting protein-mediated necrosis. Mol. Cell. Biol. **26:**2215–2225.
63. **Upton, J. W., W. J. Kaiser, and E. S. Mocarski.** 2010. Virus inhibition of RIP3-dependent necrosis. Cell Host Microbe **7:**302–313.
64. **Vandenabeele, P., W. Declercq, F. Van Herreweghe, and T. Vanden Berghe.** 2010. The role of the kinases RIP1 and RIP3 in TNF-induced necrosis. Sci. Signal. **3:**re4.
65. **Vandenabeele, P., L. Galluzzi, T. Vanden Berghe, and G. Kroemer.** 2010. Molecular mechanisms of necroptosis: an ordered cellular explosion. Nat. Rev. Mol. Cell Biol. **11:**700–714.
66. **Vercammen, D., et al.** 1998. Inhibition of caspases increases the sensitivity of L929 cells to necrosis mediated by tumor necrosis factor. J. Exp. Med. **187:**1477–1485.
67. **Vercammen, D., et al.** 1998. Dual signaling of the Fas receptor: initiation of both apoptotic and necrotic cell death pathways. J. Exp. Med. **188:**919–930.
68. **Wang, L., F. Du, and X. Wang.** 2008. TNF-alpha induces two distinct caspase-8 activation pathways. Cell **133:**693–703.
69. **Wang, X.** 2001. The expanding role of mitochondria in apoptosis. Genes Dev. **15:**2922–2933.
70. **White, C., et al.** 2005. The endoplasmic reticulum gateway to apoptosis by Bcl-X(L) modulation of the InsP3R. Nat. Cell Biol. **7:**1021–1028.
71. **Youle, R. J., and A. Strasser.** 2008. The BCL-2 protein family: opposing activities that mediate cell death. Nat. Rev. Mol. Cell Biol. **9:**47–59.
72. **Zhang, D. W., et al.** 2009. RIP3, an energy metabolism regulator that switches TNF-induced cell death from apoptosis to necrosis. Science **325:**332–336.